JOURNAL OF GEOPHYSICAL RESEARCH, VOL. 98, NO. D4, PAGES 7199–7218, APRIL 20, 1993

A Three-Dimensional Modeling Study of Trace Species in the Arctic Lower Stratosphere During Winter 1989-1990

M. P. CHIPPERFIELD,[1] D. CARIOLLE, AND P. SIMON

Météo-France, Centre National de Recherches Météorologiques, Toulouse, France

R. RAMAROSON

Office National d'Etudes et de Recherches Aérospatiales, Châtillon, France

D. J. LARY

Centre for Atmospheric Science, University of Cambridge, Cambridge, England

A three-dimensional (3D) radiative-dynamical-chemical model has been developed and used to study the evolution of trace gases in the Arctic lower stratosphere during winter 1989-1990. A series of 10-day model integrations were performed throughout this period. The model includes a comprehensive scheme of gas phase chemical reactions as well as a parameterization of heterogeneous reactions occurring on polar stratospheric cloud (PSC) surfaces. An important element of a 3D chemical model is the transport scheme. In this study the transport of chemical species is achieved by a non diffusive method well suited to the preservation of sharp gradients. During the winter studied temperatures were cold enough for the formation of both type I and type II polar stratospheric clouds from early December to early February. Model simulations in late December show that inside the polar vortex air is rapidly processed by polar stratospheric clouds converting HCl and $ClONO_2$ to active chlorine. The possibility of ozone destruction depends strongly on the amount of sunlight. In early February an average ozone loss of 15 ppbv (parts per billion by volume) /day is predicted in PSC-processed air at 50 hPa, giving a column loss of just under 1 DU/day. This loss increases to 25 ppbv/day if PSCs persist until March with a column loss of around 1.5 DU/day. The relatively small magnitude of the ozone loss predicted in the model, compared to the variability of ozone induced by dynamics, highlights the problems in identifying the signature of chemical ozone loss in the Arctic. In future years significant ozone depletion could occur if PSCs persist until late March. The efficiency of the catalytic cycles responsible for the ozone loss has been analyzed as a function of latitude, altitude and time. In general, the cycle involving ClO + ClO is the dominant loss mechanism in the polar lower stratosphere. Cycles involving BrO can make a relatively large contribution early in the season and when the levels of ClO are low. The cycle initiated by ClO + O destroys ozone at altitudes above 30 hPa but the loss is compensated, to some extent, by in situ ozone production. The results for trace species are validated, where possible, by comparison with the available measurements, although the sparse nature of the observations does not effectively constrain the model.

1. INTRODUCTION

It is now well established that the springtime ozone depletion observed over Antarctica is caused by reactions of the surface of polar stratospheric clouds (PSCs) altering the normal gas-phase partitioning of odd nitrogen (NO_y) and odd chlorine (ClO_y) species. This enables catalytic cycles involving ClO and BrO radicals to efficiently destroy ozone [see, for example, *Solomon*, 1990]. Of prime concern now is the extent to which similar processes could occur over the Arctic during winter and spring. The north polar vortex is more dynamically disturbed than its southern counterpart giving warmer temperatures and therefore less opportunity for PSCs to form. Also, the northern hemisphere vortex breaks down earlier, preventing ozone depletion from occurring significantly into the spring season. However, the azonal nature of the circulation permits air which has experienced cold temperatures at the center or edge of the vortex to experience significant exposure to sunlight.

The interest in the chemistry of the Arctic stratosphere has prompted many measurement campaigns. In January and February 1989 the Airborne Arctic Stratospheric Experiment (AASE) employed two aircraft to make measurements of several trace species (e.g., see *Geophysical Research Letters* volume 17, number 4, March supplement 1990). The following year the CHEOPS III (Chemistry of Ozone in the Polar Stratosphere III) campaign [*Pommereau and Schmidt*, 1991] made balloon-borne and ground-based observations from Scandinavia and Greenland. These campaigns showed that the chemistry of the Arctic lower stratosphere was perturbed in a similar way to the Antarctic with, for example, high levels of ClO. Thus the north polar vortex was considered as being "primed" for ozone destruction and, although no large-scale ozone loss was observed, localized depletion of around 0.4% per day has been reported [e.g., *Schoeberl et al.*, 1990, *Salawitch et al.*, 1990].

Kaye et al. [1991] and *Douglass et al.* [1991] used a three-dimensional (3D) transport model, with a parameterization of the chemistry of HCl, to investigate chemical processing by PSCs. They studied the winters of 1979 and 1989 using assimilated meteorological data and concluded that the transport of processed air, as signalled by perturbed HCl, to mid-latitudes was limited. *Granier and Brasseur*

[1]Now at Centre for Atmospheric Science, University of Cambridge, U.K.

Paper number 92JD02977.
0148-0227/93/92JD-02977$05.00

[1991] used a mechanistic 3D model with a fairly detailed chemistry scheme to investigate the potential for large-scale ozone loss over the Arctic. They applied a climatological forcing to their model and investigated the effects of interhemispheric differences in dynamics on the potential for an ozone loss over the north pole. In this study, rather than using climatological winds, we have used a 3D radiative-dynamical-chemical model to investigate trace species distributions and chemical ozone destruction by performing "real case" studies of the Arctic lower stratosphere during winter 1989-1990. We have used a model with a more detailed chemistry scheme and where possible we have validated it against the available observations. We have attempted to make the model as well suited as possible to the short-term (10-day) integrations by paying particular attention to the initialization of the model meteorological and chemical fields.

During the northern winter of 1989/1990 the midwinter period was extremely cold with temperatures in the polar lower stratosphere below the seasonal average [*Naujokat et al.*, 1990]. There was a minor warming in early December but it did not have a significant effect on temperatures inside the polar vortex. Temperatures remained cold throughout January and into February followed by a stratospheric warming which did not break down the polar vortex. The final warming was late, with the temperature gradient finally reversing in mid April. Figure 1 plots the minimum temperature in the ECMWF (European Centre for Medium Range Weather Forecasts) analyses between 50°N and the pole at the 30 hPa and 50 hPa levels from November 1989 to April 1990. Also indicated are the temperatures below which type I and type II PSCs are believed to form. The Figure shows that type I PSCs would have begun to form in mid December at these two altitudes and persisted throughout the cold midwinter period until early February. Type II PSCs could have formed in late January and early February. After the pronounced minor warming around February 10 the possibility of PSC formation is greatly reduced. Temperatures at 30 hPa remain at least 5 K above the type I PSC formation temperature. At lower levels (50 hPa and below) type I PSCs may have briefly formed in mid February and mid March. Whilst the ECMWF analyses capture the large-scale features of the lower stratospheric temperature field they often miss small, localized temperature variations. Notably, orographic forcing and adiabatic cooling of air passing over the Scandinavian mountain range can cause temperatures cold enough for PSCs which are not revealed in the ECMWF analyses.

During a series of balloon flights from January 8 to the February 8 1990, *Hofmann and Deshler* [1991] measured the ozone profile above Kiruna (68°N, 21°E). From their data, they inferred that chemical ozone destruction had occurred at around 22 km during this period. First, from the January 12 to 19 January an "episodic" loss of 1 ppmv (parts per million by volume) (140 ppbv (parts per billion by volume) /day) occurred between 22 and 26 km followed by a gradual reduction of around 20 ppbv/day throughout late January and early February. Similarly *Koike et al.* [1991] used balloon-borne measurements of ozone from Kiruna to estimate the magnitude of chemical depletion observed in January and February 1990. They concluded that ozone destruction of 0.8% per day occurred on the 525 K isentropic surface between January 18 and February 4 inside the vortex, which coincided with temperatures cold enough for type I PSC formation. In the latter part of this period, after January 26, the estimated loss rate was 1.5% per day (48 ppbv/day).

Lefèvre et al. [1991] and *Riishojgaard et al.* [1992] used a general circulation model (GCM) with a parameterization of the gas phase chemistry of ozone to study the type II

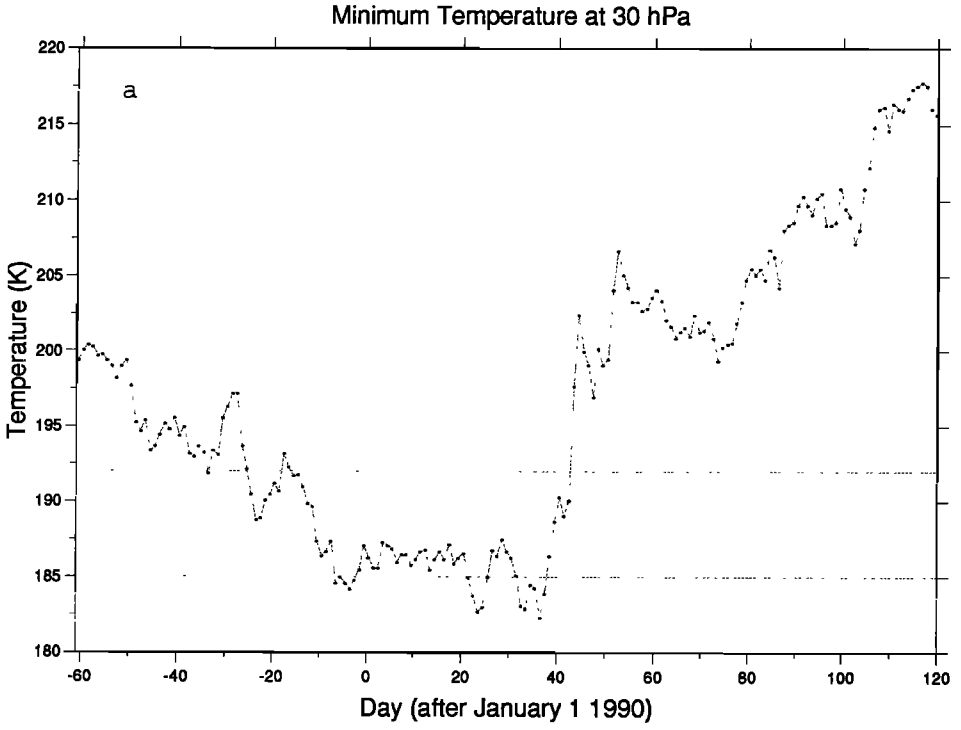

Fig. 1*a*. Minimum temperature (K) in the ECMWF analysis at 30 hPa between 50°N and 90°N from November 1989 to April 1990. Also indicated are the temperatures below which type I and type II PSCs form.

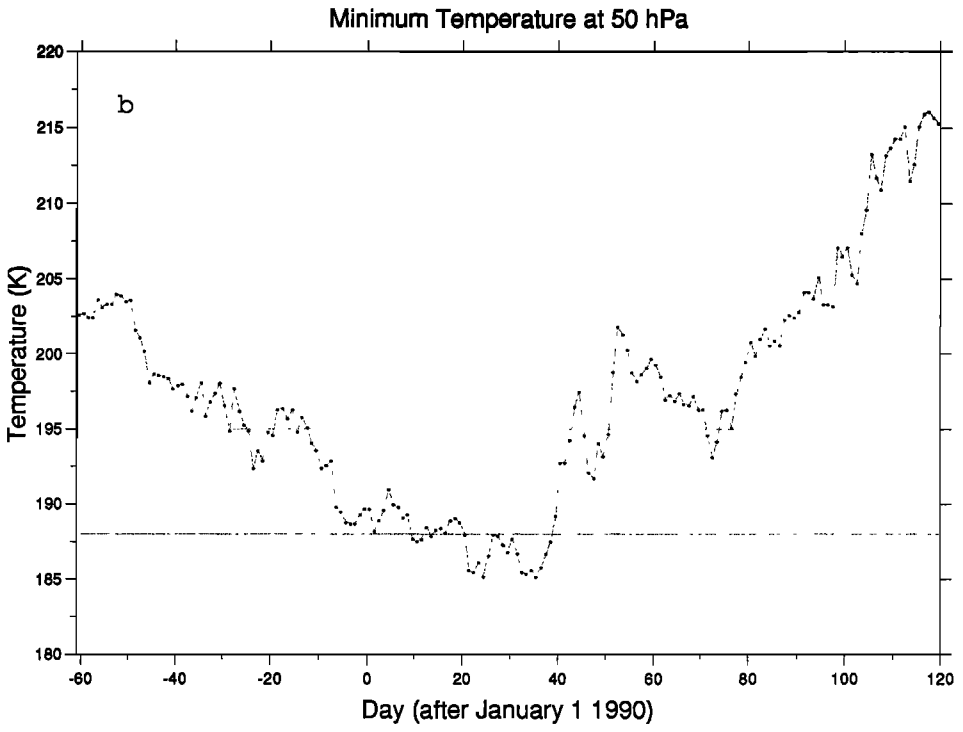

Fig. 1*b*. Same as Figure 1a but for 50 hPa.

PSC event of early February 1990 using TOMS (Total Ozone Mapping Spectrometer) data to derive the initial model O_3 field. By employing tracers to indicate the amount of time air had spent in sunlight and in the presence of type II PSCs, and comparing the evolution of the model column ozone field with TOMS data, *Lefèvre et al.* [1991] inferred that substantial ozone loss of 50 DU in 3 days (equivalent to a 40% loss at 18 km) occurred in air which had been processed by the type II PSC and had spent 16 hours in sunlight.

In our study we have used a three-dimensional chemical transport model (CTM) which uses winds derived from a GCM. The CTM has a detailed chemical scheme involving the O_x, HO_x, NO_y, ClO_y and BrO_y families and a parameterization of heterogeneous reactions on PSCs. The transport of tracers is achieved using the second order moments scheme of *Prather* [1986] which is well suited to the preservation of strong species gradients. We have performed a series of 10-day experiments spread throughout the winter of 1989-1990 to study the evolution of ozone and other trace gases. The model results are validated, where possible, by comparison with the available measurements, and the magnitude of ozone loss predicted has been analysed in terms of the chemical cycles responsible. Our model experiments for early February 1990 allow us to investigate the conclusions of *Lefèvre et al.* [1991] further, using a chemical 3D model, by examining the extent to which PSC processing may have lead to chemical ozone destruction during this period. The results of our model simulations are presented below. First, section 2 describes the Emeraude general circulation model and the chemical transport model, including the treatment of PSCs, which have been used. Section 3 describes the initialization of the model with the meteorological analysis and two-dimensional (2D) model chemical fields transformed into the coordinates of potential temperature and potential vorticity. The results of the experiments are presented in section 4, and the conclusions are summarized in section 5.

2. The Models

2.1. The "Emeraude" GCM

In this study we have used the tropospheric-stratospheric version of the "Emeraude" GCM described by *Cariolle et al.* [1990]. The model extends from the ground to about 80 km using a hybrid sigma-pressure coordinate scheme. In the lower stratosphere the vertical resolution is about 1.8 km. The model contains a full description of the main physical processes such as radiative transfer and the hydrological cycle. This spectral model has been used in the horizontal resolution of T21, i.e., allowing a maximum total wavenumber of 21 in the horizontal. The Gaussian grid corresponding to this truncation has a resolution of 5.6° in longitude and latitude. The model uses a leapfrog integration scheme with a 30-min time step. An integration of the GCM is performed to generate wind and temperature fields which are stored every 6 hours and used to force the CTM.

2.2. Chemical Transport Model

The chemical transport model uses the same grid as the GCM which, for the experiments described here, is the Gaussian grid corresponding to the T21 spectral resolution. The method by which tracers are transported is critically important in coupled chemical-dynamical models. This is especially true for studies of the polar lower stratosphere where localized PSC processing can lead to strong inhomogeneities in a tracer's distribution. In our CTM the chemical tracers are advected using the transport scheme of *Prather* [1986] in three dimensions which conserves the second-order moments of the tracer distribution. This scheme has been used, in preference to the spectral transport scheme of the GCM, as it is less diffusive and better able to represent the strong gradients in species distribution that can be found, for example, at the edge of the polar vortex. The use of

the Prather scheme has resulted in a large improvement in the model compared to a previous version which used the spectral scheme.

The photochemical package which has been coupled to the CTM is based on a photochemical box model, developed by *Ramaroson* [1989] and *Ramaroson et al.* [1990, 1992]. The model uses the semi-implicit symmetric (SIS) method to integrate the chemical continuity equations. Effectively, this box model is called at every model grid point and the chemical changes calculated are added to the mean tracer distribution (zeroth-order moment) of the Prather scheme in each box, splitting the effects of chemistry and dynamics (the first- and second-order moments of the tracer distribution are not modified by the chemistry). For this study the photochemical model of *Ramaroson et al.* [1990] has been updated as follows. The chemical species O, O_3, H_2O_2, OClO, Cl_2O_2, Br, BrO, $BrONO_2$ and BrCl have been added to make the model appropriate for the study of polar stratospheric chemistry. Table 1 lists the transported chemical species in the model and the HO_x species which are assumed to be in steady state. Note that in the model the chemical families NO_y, ClO_y and BrO_y have no sources or sinks, which is a satisfactory approximation to make in the lower stratosphere for simulations of 10 days or so. The mixing ratio of H_2O is obtained from the water vapor tracer of the GCM. In addition, fixed zonal mean fields of CH_4 and CO, taken from the 2D model of *Cariolle and Brard* [1984], are used. The distribution of CH_4 is necessary to determine the recovery of ClO_y species after heterogeneous processing. The model uses the family approach for certain short-lived species (e.g., O + O_3, Cl + ClO + Cl_2O_2, Br + BrO, NO + NO_2 + NO_3). These species rapidly establish photochemical equilibrium during daylight and the use of these families does not prevent the partitioning of species during darkness. This has the advantage that the concentration of each species is calculated at every location, which is important when considering localized sources and sinks of species due to reactions on PSC surfaces. When studying the polar lower stratosphere, the calculation of photolysis rates is an important consideration. For this study we have used the "look-up table" scheme of *Lary and Pyle* [1991] which is both computationally efficient and able to calculate photolysis rates for zenith angles up to 96°. This scheme does not use the model calculated O_3 field in the calculation of the optical depth but instead uses a standard mid-latitude O_3 profile. The photochemical data is taken from *DeMore et al.* [1990]. The absorption cross sections for BrCl were obtained from R. A. Cox (personal communication, 1988). For the photolysis of HNO_3 the temperature dependent cross sections of *Rattigan et al.* [1992] were used. The time step used in the CTM is 30 min for the dynamics and 15 min for the chemistry. Although the chemistry scheme is stable for longer time steps a short time step was chosen so that the diurnal cycle of species could be adequately resolved.

In addition to these improvements in the chemical scheme a treatment of heterogeneous processes, occurring on the surface of polar stratospheric clouds, has been included in the model. The scheme does not contain any detailed microphysics but it does distinguish between type I and type II clouds. For type I PSCs the model temperature and mixing ratios of H_2O and HNO_3 are used, together with the algorithm of *Hanson and Mauersberger* [1988a], to predict when these PSCs are thermodynamically possible and the resultant equilibrium gas phase mixing ratio of HNO_3. The condensed particles of $HNO_3.3H_2O$ (nitric acid trihydrate - NAT) are assumed to have a radius of 1 μm, which is used in the calculation of the available surface area. For type II PSCs the model temperature field and water vapor is used in conjunction with the Tetens equation [*Murray*, 1967], which describes the saturation vapor pressure of water over ice, to predict their occurrence. Similarly, when type II PSCs are thermodynamically possible, the amount of ice condensed is assumed to be in particles of radius 10 μm. When formed, these type II particles are sedimented with a speed of 1.5 km/day, consistent with a size of 10 μm. The sedimented PSC particles are deposited in the model level below. HCl is incorporated into the PSCs in the mole fractions given by *Hanson and Mauersberger* [1988b]. When the PSCs evaporate the condensed species are returned to the gas phase. Once PSCs have been formed in the model, the following five reactions are assumed to occur on the particle surfaces:

$$\text{(R1)}\quad N_2O_5(g) + H_2O(s) \rightarrow 2HNO_3(s)$$
$$\text{(R2)}\quad N_2O_5(g) + HCl(s) \rightarrow ClNO_2(g) + HNO_3(s)$$
$$\text{(R3)}\quad ClONO_2(g) + H_2O(s) \rightarrow HOCl(g) + HNO_3(s)$$
$$\text{(R4)}\quad ClONO_2(g) + HCl(s) \rightarrow Cl_2(g) + HNO_3(s)$$
$$\text{(R5)}\quad HOCl(g) + HCl(s) \rightarrow Cl_2(g) + H_2O(s)$$

The reaction probabilities (γ) for these reactions are taken from experimental data and the values used are given in Table 2 for the two types of PSC (see *World Meteorological Organisation/ UNEP* [1991] for a discussion of these values). Reaction (R4) is believed to involve the two step process of reaction (R3) followed by reaction (R5) [*Abbatt et al.*, 1992]. Therefore for reaction (R5) the same values of γ were employed as for reaction (R4). The rate of chemical reaction is calculated by using the measured reaction probabilities listed in Table 2 along with the calculated PSC surface area and the mean kinetic speed of the gaseous molecules [see, e.g., *Rodriguez et al.*, 1989]. These reactions are treated as first-order loss reactions for the gaseous molecule unless the concentration of condensed HCl would limit this rate. Note that in order to maintain the computational efficiency of the model the chlorine products of reactions (R2), (R4) and (R5) are given in terms of Cl and NO_2. In the stratosphere any Cl_2 and $ClNO_2$ formed will be rapidly photolyzed in the presence of sunlight. In the dark the Cl produced in the model by the heterogeneous reactions will be instantaneously converted to ClO and Cl_2O_2 within the model ClO_x family. With the adopted parameterization type II PSCs, when they occur, will provide faster heterogeneous

TABLE 1. Chemical Species Contained in the Model

Transported	Not transported
O_x (= O_3 + $O(^3P)$ + $O(^1D)$), H_2O_2	
NO_x (=NO + NO_2 + NO_3),N_2O_5, HNO_3,HO_2NO_2,	HO_x (= H + OH + HO_2)
ClO_x (=Cl + ClO + $2Cl_2O_2$),$ClONO_2$,HCl,HOCl,OClO,	
BrO_x (=Br + BrO),$BrONO_2$,BrCl	

TABLE 2. Reaction Probabilities for Heterogeneous Reactions

Reaction	Reaction Probability (γ)	
	Type I	Type II
(R1)	0.0006	0.03
(R2)	0.003	0.03
(R3)	0.006	0.3
(R4)	0.3	0.3
(R5)	0.3	0.3

rates than type I PSCs. First, the γ values for the type II particles are equal to or larger than those for type I particles. Second, type II PSCs will provide a larger surface area per unit volume with the particle sizes adopted. In addition, type II PSCs will also perturb the atmosphere by the permanent removal of NO_y by sedimentation.

We have attempted to make the parameterization of PSCs and the associated heterogeneous reactions as realistic as possible without using a detailed microphysical model. However, there still exist a number of uncertainties. These include the variation of γ as a function of particle composition, the size distribution of particles expected under Arctic cooling conditions and the onset temperatures of the formation of type I PSCs. Heterogeneous reactions occurring on the background sulphate aerosol layer are not included in this study. (Note that by using LIMS (Limb Infra red Monitor of the Stratosphere) data for the initialization of HNO_3 we have implicitly accounted for the effects of reaction (R1) on the background aerosol.)

3. Initialization

For the experiments performed here the GCM was initialized from the meteorological analysis of the ECMWF (European Centre for Medium Range Weather Forecasts) for the appropriate day. This analysis gives the initial fields of the temperature, winds and water vapor below 10 hPa. The initial conditions for the nine model levels located above 10 hPa were taken from climatology.

The species in the CTM were initialized from fields taken from an updated version of the 2D model of *Harwood and Pyle* [1975]. However, this 2D model in common with others has a few notable shortcomings at high latitudes. First, during the winter at northern high latitudes 2D models which contain only gas phase chemistry underestimate the abundance of HNO_3 when compared to LIMS data, probably due to the omission of reaction (R1) above [*Austin et al.*, 1986], although problems at mid-latitudes may still remain [*Rood et al.*, 1990]. Therefore the 2D model field of HNO_3 was constrained to agree with the LIMS (Limb Infra-red Monitor of the Stratosphere) monthly mean data for January 1979 by including the effects of reaction (R1). Second, 2D models appear to underestimate the degree of descent observed over the poles. This implies, for example, that these models will underestimate the abundance of inorganic chlorine (and overestimate, e.g., CH_4) in the polar lower stratosphere. This is an important factor in determining the potential for ozone depletion at high latitudes and accordingly the initial 2D model field of ClO_y was constrained to agree with the estimates of the total inorganic chlorine at 44°N and 67°N by *Schmidt et al.* [1991] based on their measurements of long-lived tracers. The 2D model field of inorganic bromine (BrO_y) was constrained in a similar way. In the model runs presented here the abundance of ClO_y and BrO_y was 3.2 ppbv and 12 pptv (parts per trillion by volume) respectively, in the upper stratosphere.

For short integrations of a 3D model the quality of the simulation depends critically on the initialization of the chemical fields. Traditionally, zonal mean fields from 2D models have been used. However, during the northern winter the atmosphere can be highly non zonal. Therefore in this study we have attempted to initialize the chemical fields in as realistic a way as possible by introducing the azonality of polar vortex into the species distributions. This we have done by initializing the fields in the north polar lower stratosphere using the coordinates of potential vorticity (PV) and potential temperature (θ). *Douglass et al.* [1990] described the construction of global 3D fields in these coordinates using 2D model data. A similar procedure was adopted here.

The initial 3D model chemical fields were zonal mean fields interpolated directly from the 2D model fields except polewards of 30°N between 200 hPa and 10 hPa. In this region the model fields of the longer-lived and more abundant species were initialized using potential vorticity and potential temperature. The zonal mean fields of potential temperature and potential vorticity were calculated from the 2D model temperature field and these were used to map the constituent mixing ratios onto the 3D model grid using the PV and θ at each grid point. Thus the model fields were constrained to follow the morphology of the polar vortex, which, during this period, was highly non zonal. This is illustrated in Figure 2 which shows PV and HNO_3 on the 500 K isentropic surface on February 4th, the initial day of model run C (below). The PV map (Figure 2a) shows the distorted nature of the polar vortex, with it displaced off of the pole towards northern Europe. The HNO_3 field (Figure 2b) mimics the distribution of PV. The HNO_3 distribution has weak horizontal gradients at mid-latitudes and in the center of the vortex separated by strong gradients in mix-

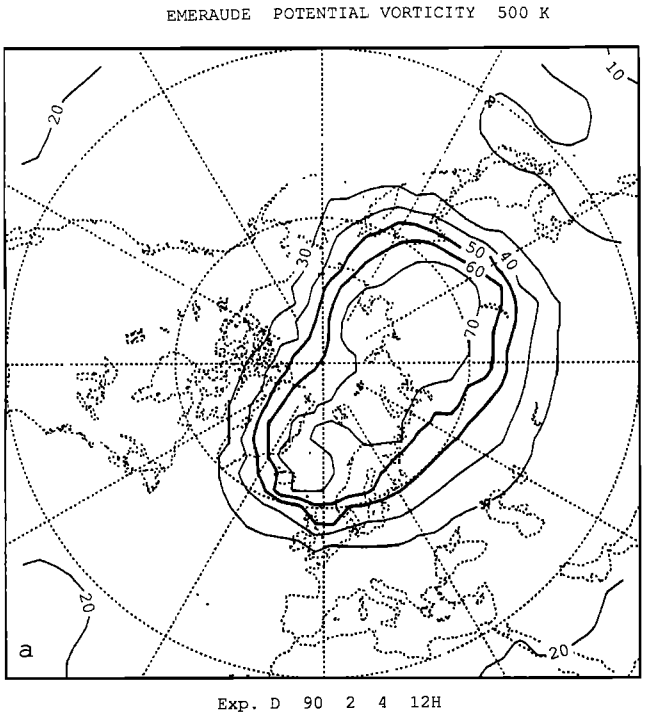

Fig. 2*a*. Ertel's potential vorticity (x10^6 K m^2 s^{-1} kg^{-1}) on the 500 K isentropic surface at 1200 UT on February 4. Contour interval is 10x10^6 K m^2 s^{-1} kg^{-1}.

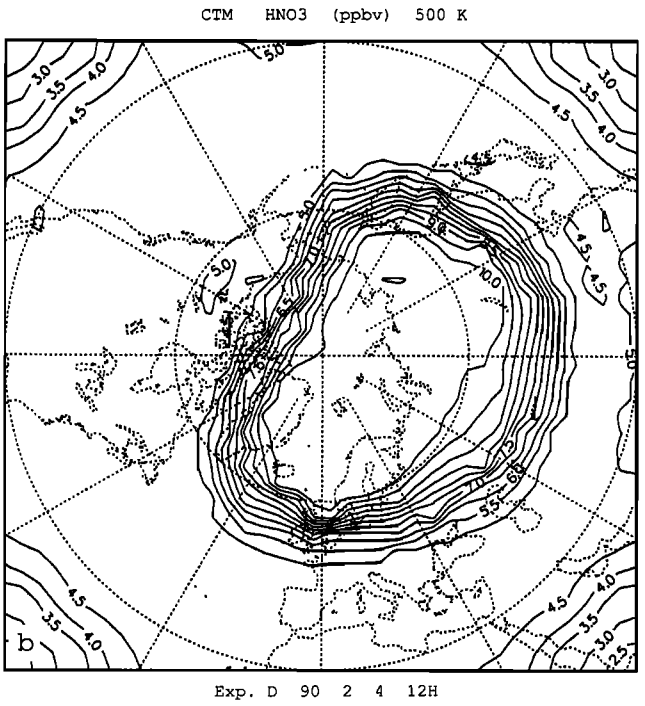

Fig. 2*b*. Mixing ratio of HNO_3 (ppbv) on the 500 K isentropic surface at 1200 UT on February 4 from run D. Contour interval is 0.5 ppbv.

ing ratio around the edge of the vortex. The distribution of HNO_3 around the 60° latitude circle illustrates the azonal nature of the field, with values ranging from less than 5 ppbv to more than 10 ppbv. Note that the HNO_3 field was constructed by using a direct correlation between the zonal mean PV calculated from the 2D model and the PV calculated in the 3D model. It is to be expected that the zonal mean PV from the 2D model will not show values as large as those observed at the center of the polar vortex. This results in the large, featureless area inside the polar vortex. In experiments C, D, E and F (see below) TOMS data was used to initialize the model ozone field using the method of *Riishojgaard et al.* [1992]. Finally, the shorter-lived chemical species in the model were "balanced" by performing a 2-day integration of the CTM without transport and a constant temperature field. This was to ensure that at the start of the model run proper these shorter-lived species had been brought into equilibrium with the local temperature and photolysis fields. During this 2-day integration the heterogeneous reactions described above were included where appropriate. Thus at the start of the experiment itself the air in the presence of the PSCs had already been perturbed. In addition, because LIMS HNO_3 data was used in the initialization procedure the partitioning of NO_y species had been perturbed all over the polar region from that expected on the basis of gas phase chemistry. For some experiments later in the winter, as described below, some preprocessing of chlorine species was assumed.

4. Results

A series of 10-day model integrations were performed over the winter period. Runs A and B both started on the December 25 1989, shortly after the temperatures in the vortex were cold enough to permit the formation of PSCs (Figure 1). Run A and run B differ only in that run A did not contain heterogeneous chemistry while run B did. Two further runs (C and D) were initialized on the February 4 1990. In run D we assumed that prior to this date air in the polar vortex had been processed by PSCs converting HCl and $ClONO_2$ to active chlorine. During early February the polar vortex was displaced over Scandinavia with very cold temperatures (cold enough for the formation of type II PSCs, Figure 1) in the lower stratosphere. The position of the vortex enabled air which had been processed by PSCs to undergo exposure to sunlight. As shown in Figure 1, early February provided the latest opportunity for significant PSC activity. However, to examine the potential for ozone depletion in winters where the temperatures remain cold until later in the year, two experiments (E and F) were performed using the same initial conditions and dynamical forcing as experiments C and D but with the solar position advanced by one month giving photolysis conditions appropriate for early March. The model runs performed are summarized in Table 3.

4.1. Meteorological Forecast and PSCs

The simplified treatment of PSCs contained in the model assumes that PSCs occur whenever they are thermodynamically possible. Therefore as there is no barrier to nucleation, the predicted area of PSCs will represent an upper limit. However, this will be offset slightly because, as noted above, the temperature forecast of the model differs from observations by a few degrees. Notably, the model does not produce the very cold temperatures in or near the polar vortex caused by orographic forcing and adiabatic ascent. Figure 3 shows the predicted occurrence of PSCs at 50 hPa on February 5th from experiment D. At this altitude the extent of the type I PSC approximately follows the 194 K temperature contour and the type II PSC the 190 K contour. Figure 4 is a latitude cross section at 33.75°E showing the occurrence of type I and type II PSCs in the stratosphere (ice saturation also occurs in the troposphere but is not shown). Type I PSCs occur polewards of 60°N between 20 and 100 hPa. (Interestingly, type I PSCs are also predicted at the equator although, in the model, the heterogeneous chemical reactions are not activated there.) Type II PSCs occur between 60°-80°N and 70-30 hPa.

In our experiments the GCM, whose winds are used to force the CTM, is used in the resolution of T21. In this low resolution the GCM forecast will diverge from reality and cannot be expected to completely capture the observed synoptic forcing. For example, in the experiments initialized on February 4 the GCM does not faithfully reproduce the pronounced minor warming which occurred around February 8.

TABLE 3. Model Runs Performed

Run	Start Date	Heterogeneous Chemistry	Comments
A	Dec. 25 1989	no	
B	Dec. 25 1989	yes	
C	Feb. 4 1990	no	
D	Feb. 4 1990	yes	
E	Feb. 4 1990	no	Solar position early March
F	Feb. 4 1990	yes	Solar position early March

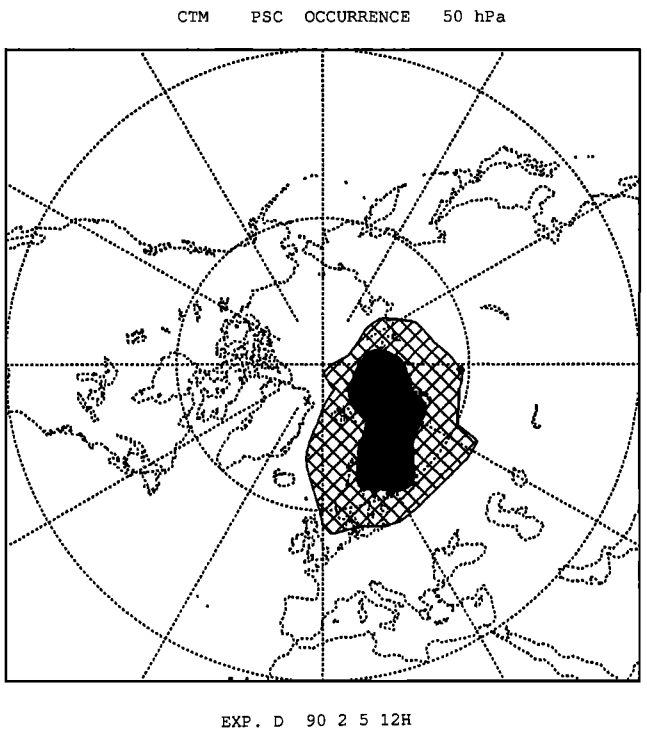

Fig. 3. The occurrence of type I (hatched shading) and type II (solid shading) PSCs at 50 hPa at 1200 UT on February 5 from run D.

4.2. *Chemical Species*

Results are presented here for trace chemical species. Where possible the model values are compared to observations made during the CHEOPS III campaign and also measurements from the AASE mission which will be representative of the chemistry of the Arctic lower stratosphere. The measurements serve to validate the model but are generally too sparse to effectively constrain its behavior.

Nitrogen species. Pommereau et al. [1991] measured the vertical column of NO_2 with UV-visible spectrometers at two sites during January and February 1990. One spectrometer was located at Sondre Stromfjord (67°N, 51°W) and the other at Kiruna (68°N, 21°E). At Sondre Stromfjord the observed twilight vertical column of NO_2 in January and early February was around $1x10^{15}$ molecules cm^{-2} with the morning and evening measurements yielding similar values. During early February, coinciding with a minor warming, the measured vertical column was $1.6x10^{15}$ molecules cm^{-2} in the evening and 0.6 molecules cm^{-2} in the morning. At Kiruna the measured NO_2 column in January and February showed a baseline of around $1.4x10^{15}$ molecules cm^{-2} superimposed on which were numerous episodes of tropospheric pollution leading sporadically to a much larger column. *Adrian et al.* [1991], using infrared measurements, gave an upper limit to the vertical column of NO_2 over Es- range of $1.2x10^{15}$ molecules cm^{-2}. Figure 5a shows the NO_2 column (above 300 hPa) from run D at 1200 UT on February 6th. At 30°N the diurnal variation of NO_2 can be seen with an increase in sunset followed by a slow decay during the night and a sharp decrease at sunrise. There is a large area, covering Scandinavia, the northern Atlantic and Greenland where the NO_2 column is less than $1x10^{15}$ molecules cm^{-2}. At 50 hPa (Figure 5b) there are regions, north of 60°N between 30°E and 120°E, where the abundance of NO_2 is effectively zero due to the heterogeneous conversion of NO_x to HNO_3. The use of LIMS HNO_3 data to constrain the initial model NO_y fields results in the suppression of NO_2 values throughout the polar region. The presence of PSCs further reduces the NO_2 over northern Scandinavia.

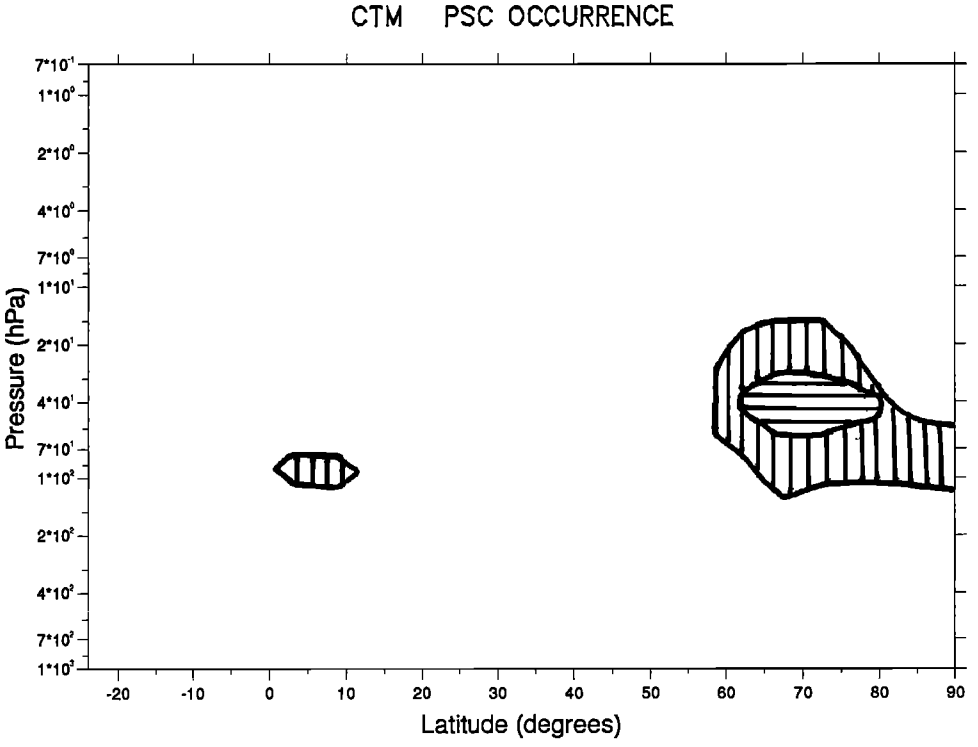

Fig. 4. The predicted occurrence of type I PSCs (vertical shading) and type II PSCs (horizontal shading) at 33.75°E at 1200 UT on February 5 from run D.

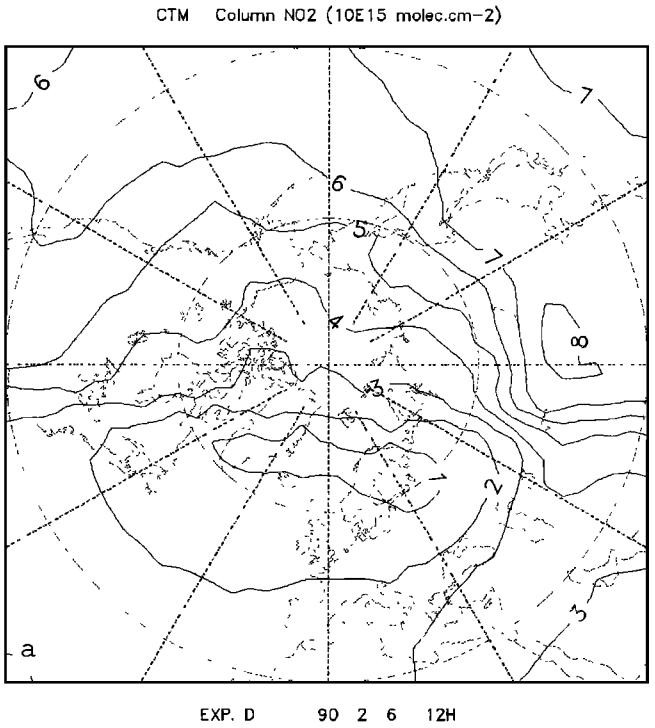

Fig. 5*a*. NO_2 column (x10^{15} molecules cm^{-2}) above 300 hPa from run D at 1200 UT on February 6.

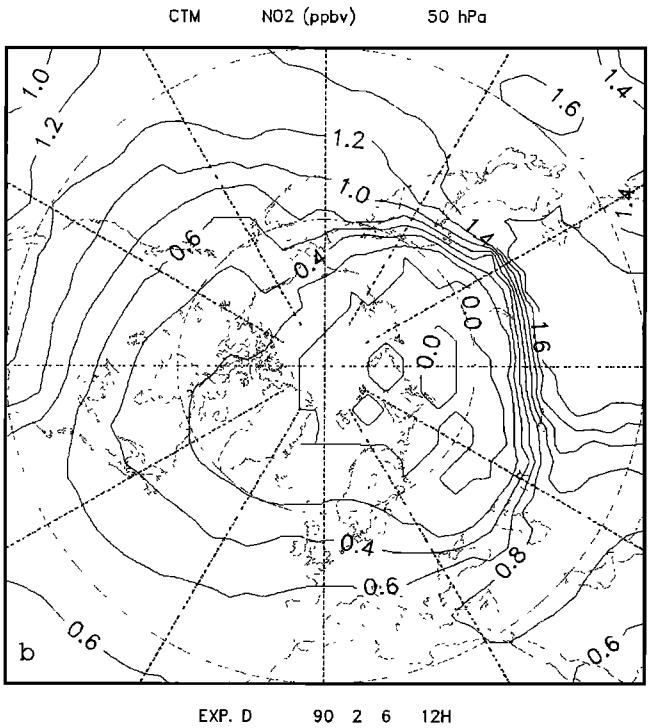

Fig. 5*b*. Mixing ratio of NO_2 (ppbv) at 50 hpa at 1200 UT on February 6 from run D. Contour interval is 0.2 ppbv.

Adrian et al. [1991] also measured the column abundance of HNO_3. In January and February 1990, above Kiruna the HNO_3 column abundance was large, being 2.9x10^{16} molecules cm^{-2}. This is consistent with the results from the AASE and in contrast to observations in the Antarctic. The column HNO_3 abundance in the model (not shown) is consistent with these observations. The column abundance is around 2.5x10^{16} throughout the polar region. The effect of using LIMS data to initialize the HNO_3 is to ensure that the majority of NO_y is contained in HNO_3 in the lower stratosphere. The mixing ratio of HNO_3 at 50 hPa on February 6 from run D is shown in Figure 6 (the quantity plotted is the total HNO_3 comprising both the gas phase and that condensed in the PSCs). The high values of HNO_3 of around 9-10 ppbv are located inside the polar vortex. However, coincident with the type II PSC (Figure 4 above) there is a local minimum with an equivalent gas phase mixing ratio of 6 ppbv. This is caused by the sedimentation of the large type II particles to lower altitudes. In these short, 10-day integrations the degree of denitrification will not significantly affect the magnitude of the ozone destruction. Essentially all of the odd nitrogen is in the form of HNO_3, whose photolysis rate is slow enough (especially when calculated using the temperature dependent cross sections of *Rattigan et al.* [1992]) to prevent the release of NO_2, thereby maintaining the levels of active chlorine. The amount of denitrification will, of course, affect the long-term recovery of an air mass [e.g. see *Prather and Jaffe*, 1990].

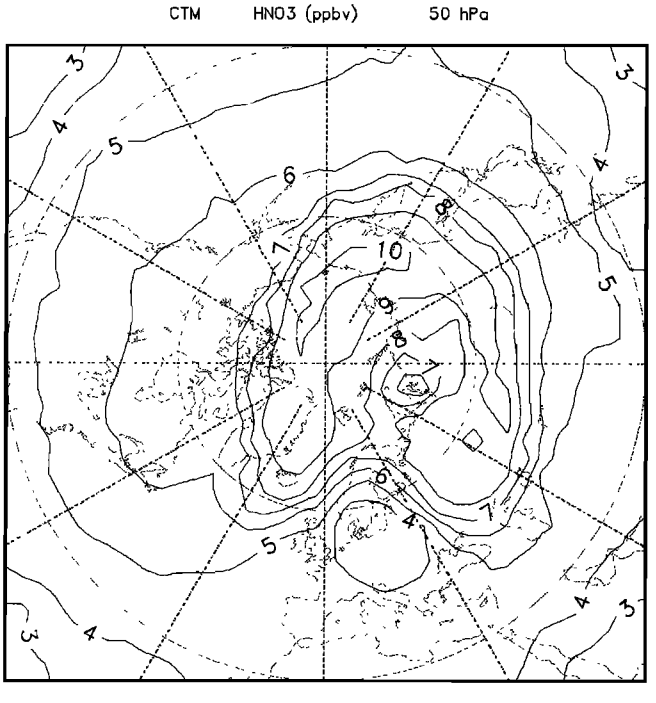

Fig. 6. Mixing ratio of total HNO3 (ppbv) at 50 hpa at 1200 UT on February 6 from run D. Contour interval is 1 ppbv.

Chlorine species. The processing of chlorine species in early winter has been investigated by a comparison of experiments A and B. Figure 7a shows the difference in HCl between these two runs on the 500 K surface on the January 4 1990, 10 days into the model integration. Figure 7b shows PV on the 500 K isentropic surface on this day. Air inside the vortex, as indicated by the strong gradients of PV, has been processed by PSCs resulting in the heterogeneous conversion of HCl to active chlorine (ClO_x). At the center of the vortex effectively all of the HCl has been converted in run B. Note the way that the HCl-poor air is confined to the polar regions and the strong gradients at the edge of the vortex, even with the comparatively low model resolution of T21. This illustrates the non diffusive

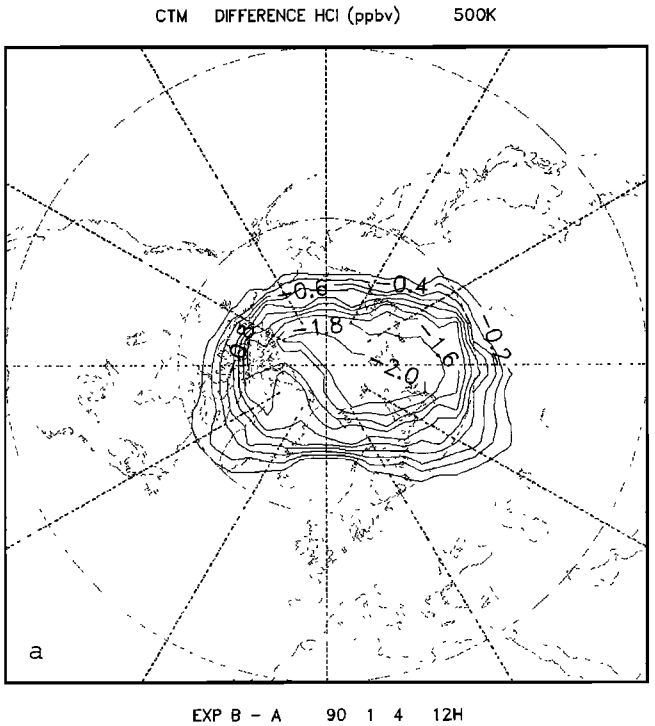

Fig. 7*a*. Difference in the HCl mixing ratio (ppbv) between run B and run A on the 500 K surface at 1200 UT on January 4. Contour interval is 0.2 ppbv.

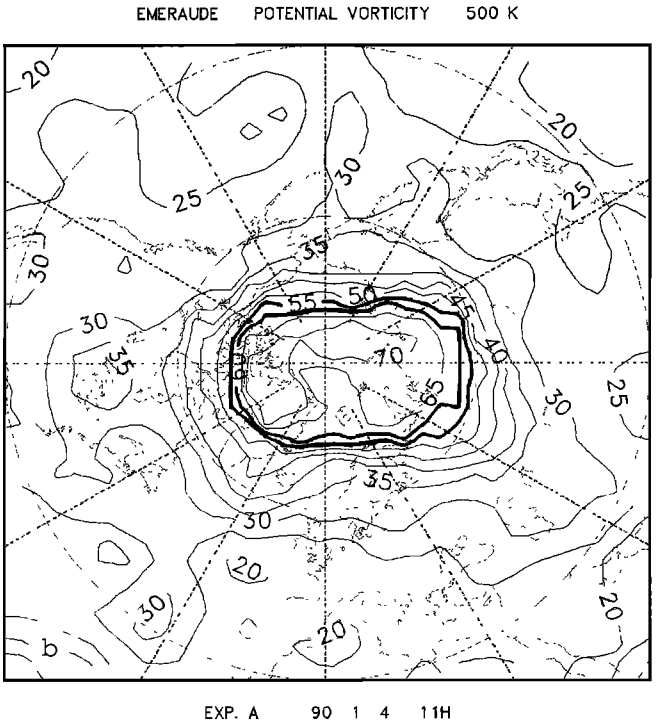

Fig. 7*b*. Ertel's potential vorticity (x10^6 K m^2 s^{-1} kg^{-1}) on the 500 K isentropic surface at 1200 UT on January 4 from run A. Contour interval is 5x10^6 K m^2 s^{-1} kg^{-1}.

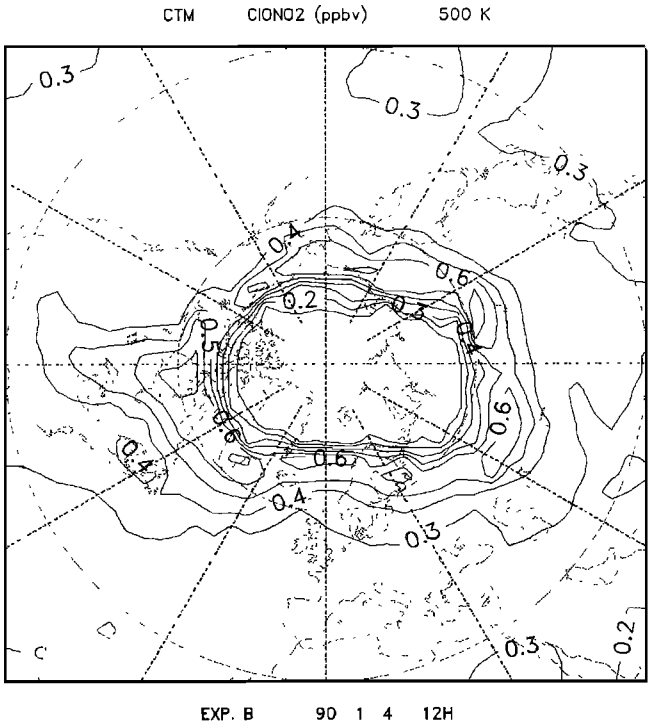

Fig. 7*c*. Mixing ratio of $ClONO_2$ from run B on the 500K surface at 1200 UT on January 4.

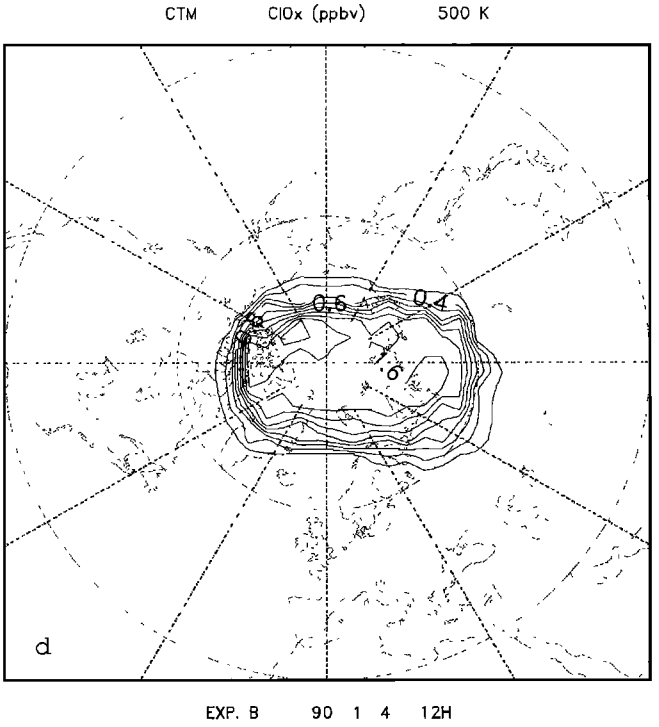

Fig. 7*d*. Mixing ratio of ClO_x from run B on the 500 K surface at 1200 UT on January 4.

nature of the Prather transport scheme. In earlier experiments we used the spectral scheme of the GCM for tracer advection. The results were far more diffusive with changes to species at high latitudes being rapidly "transported" to lower latitudes. When this lead to chemical reactions between species the model results quickly became unrealistic. For example, the Gibb's phenomenon, associated with the spectral truncation, caused polar air high in ClO to react with mid-latitude air containing NO_2 resulting in the formation of $ClONO_2$. Whilst the performance of the spectral scheme would improve at higher resolutions, the computational cost of including chemistry in a 3D model often necessitates the use of a coarse resolution. In such low resolutions the shortcomings of a transport scheme can be more evident.

The properties of various transport schemes have been well investigated in several 1D passive tracer experiments (e.g., see *Muller* [1992 and references therein]). However, when chemical interactions between tracers are considered, the problems are compounded and the results from a scheme which is too diffusive can rapidly become unrealistic.

Figure 7c plots $ClONO_2$ from run B. The minimum at the center of the vortex is partly due to loss by heterogeneous reactions on PSCs. This results in a ring of $ClONO_2$ around the pole. Note that in run B mixing at the edge of the vortex has not lead to a large increase in $ClONO_2$ compared to run A. Mixing has contributed to an increase of $ClONO_2$ of 0.2 ppbv compared to run A at 500 K. At 600 K (not shown) the effect of mixing is larger with an increase in $ClONO_2$ of 0.6 ppbv. Figure 7d shows the mixing ratio of ClO_x (=ClO + $2Cl_2O_2$) at 500 K from run B. Inside the polar vortex the mixing ratio is up to 2 ppbv reflecting the conversion of HCl and $ClONO_2$ above. These results show that by the end of December 1989, when large-scale temperatures inside the polar vortex had been cold enough for PSCs, almost complete conversion of HCl to active forms could have occurred. *Rood et al.* [1992] discussed the possibility that episodic dynamical events (which produce ozone "miniholes") can cause a significant amount of processing in December before the large-scale temperature falls below the PSC threshold. Figure 1 shows that episodic processing may have been important in early December 1989 (in as much as the ECMWF analyses capture the episodic cold temperatures) but by the end of December temperatures were continuously well below the PSC formation threshold.

The OClO molecule provides an important indication of perturbed halogen chemistry in the polar stratosphere. It is believed to be produced exclusively by the reaction

$$BrO + ClO \rightarrow Br + OClO$$

During the day OClO is rapidly photolyzed but at night its concentration can build up. *Perner et al.* [1991] measured elevated levels of OClO from January 5 to February 2, 1990, above Sondre Stromfjord (67°N, 51°W). Their results confirm the OClO observations of *Solomon et al.* [1988] in 1988 and *Schiller et al.* [1990] in 1989. *Perner et al.* [1991] measured a vertical twilight column of OClO of between 0.8 and 1.6x10^{13} molecules cm^{-2} (at 91° solar zenith angle) during January and early February. *Schiller et al.* [1990] measured a twilight vertical column of 1.0x10^{13} molecules cm^{-2} (at 88° SZA) and a nighttime column of 10x10^{13} molecules cm^{-2}. Figure 8a plots the column OClO from the model run B at 1200 UT on January 4. The OClO column is large inside the dark vortex with a maximum column of 8.0x10^{13} molecules cm^{-2}. Whilst a comparison with the twilight column measurements is difficult, the values in the model are in reasonable accord with those obtained in the presence of perturbed chemistry. The mixing ratio of OClO at 500 K on this day is 60-70pptv in the vortex as shown in Figure 8b.

Adrian et al. [1991] made infrared measurements of the column abundance of HCl from Esrange (68°N, 21°E), Sweden in January and February 1990. During January and up to February 4 the measured vertical column was around 2.5x10^{15} molecules cm^{-2}. This corresponded to an estimated stratospheric column of 2x10^{15} molecules cm^{-2}. However, the next observations, on February 8 and 9, measured much larger HCl columns of 4.8x10^{15} molecules cm^{-2}

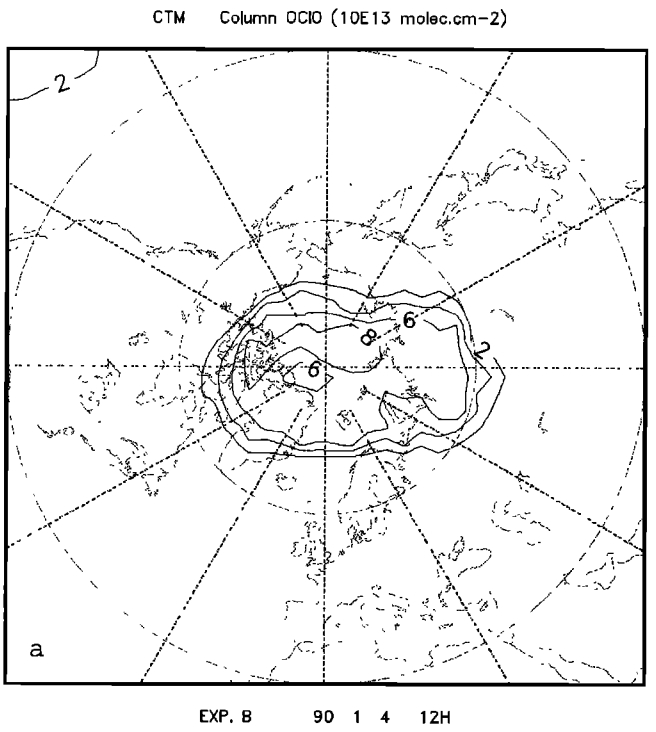

Fig. 8*a*. Column OClO (x10^{13} molecules cm^{-2}) from run B at 1200 UT on January 4.

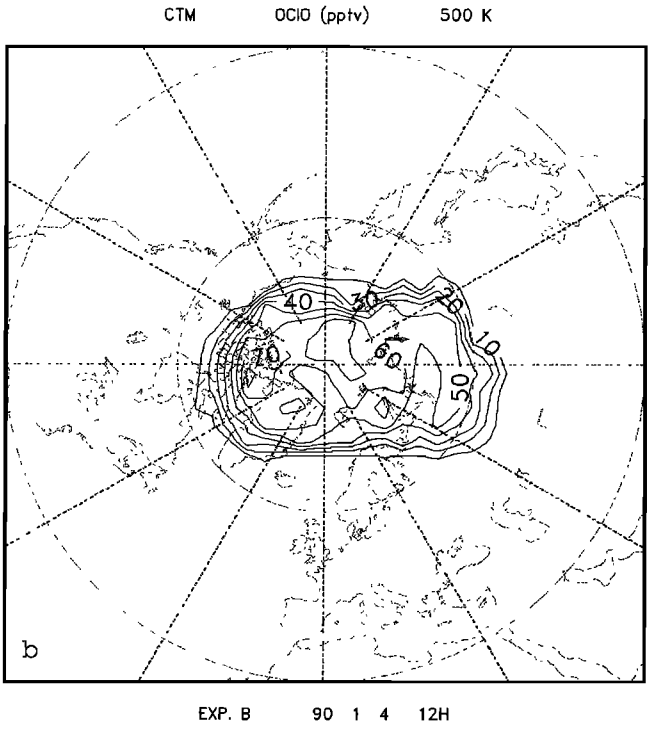

Fig. 8*b*. OClO mixing ratio (pptv) at 500 K from run B at 1200 UT on January 4.

(equivalent to a stratospheric column of 4x10^{15} molecules cm^{-2}). The increase from the 4th to the 8th of February corresponded to warmer air moving over Esrange. As *Adrian et al.* [1991] also measured the HF column, which effectively remained constant through this period, they concluded that before the 4th of February a significant fraction of the stratospheric HCl was converted to other ClO_y

species or condensed in PSC particles. Figure 9 shows the column HCl (above 300 hPa) on February 6 from run D. The quantity plotted is the total HCl, taking into account both gas phase and condensed HCl. With the PSC scheme employed in the model, the amount of HCl condensed in particles in regions with both type I and type II clouds would be equivalent to a column of around 10^{14} molecules cm^{-2}. A local minimum of around 2.0 $x10^{15}$ molecules cm^{-2} is situated to the east of Finland, coincident with the occurrence of PSCs. This is surrounded by larger column abundances of 3.5- 4.0$x10^{15}$ molecules cm^{-2} in air which has not been processed by PSCs. The large HCl column in the model of around 5.5$x10^{15}$ molecules cm^{-2} coincides with the warmest lower stratospheric temperatures. This is a consequence of the model initialization using θ as the vertical coordinate; where the atmosphere is warm the 2D model profile is descended further. An inspection of the ECMWF analyses for this period [*Riishojgaard et al.*, 1992] shows that between the 4th and the 10th of February the polar vortex shifted towards Asia and rotated clockwise. The comparison of the model results with the measurements are strongly influenced by the model initial conditions and affected by the dynamical evolution of the GCM forecast. However, the model supports the possibility that the movement of air over Kiruna and the replacement of PSC-processed air by unprocessed air could explain the increase in HCl observed by *Adrian et al.* [1991] in early February. A latitude altitude cross section of ClO at 50°E is shown in Figure 10. The region of elevated ClO in the polar lower stratosphere is clearly evident, with mixing ratios of up to 1.4 ppbv at 40-50 hPa

Thus the presence of polar stratospheric clouds severely perturbs the partitioning of inorganic chlorine species from that expected on the basis of gas phase chemistry. After PSC processing, the time scale for the recovery of this gas phase "equilibrium" is of the order of months [*McKenna et al.*, 1990]. First, as NO_2 is released by the photolysis of HNO_3 it can react with ClO to form chlorine nitrate on a time scale of a few days. Second, the recovery of HCl by reactions such as

$$Cl + CH_4 \rightarrow HCl + CH_3$$

takes place on a much longer time scale. The rate of this recovery will therefore depend on the amount of insolation and the extent of denitrification of an air parcel [*Prather and Jaffe*, 1990]. In the 3D experiments described here, mixing can also lead to the deactivation of ClO_x by the mixing of mid-latitude and polar air.

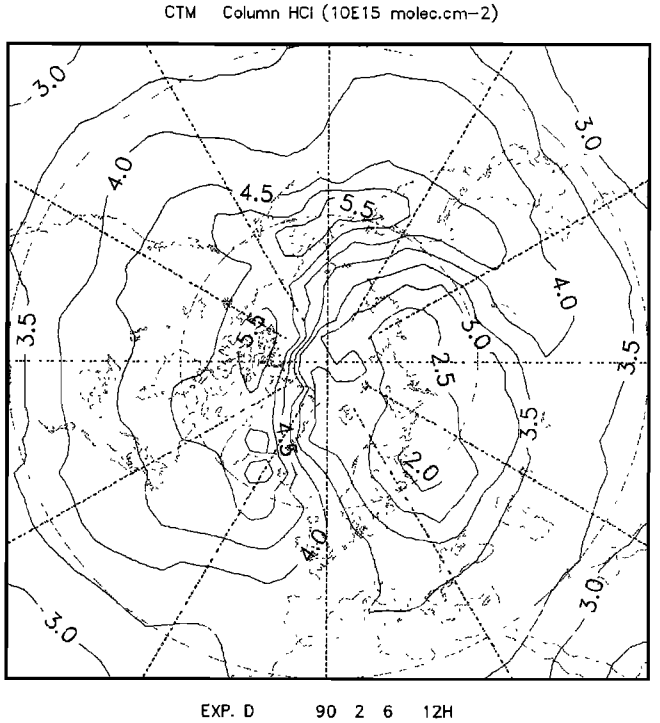

Fig. 9. HCl column ($x10^{15}$ molecules cm^{-2}) above 300 hPa from run D at 1200 UT on February 5.

Bromine species. Figure 11a plots the mixing ratio of $BrONO_2$ at 50 hPa on February 6. The "denoxification" (conversion of NO_x species to HNO_3) of the air in the presence of PSCs has lead to a large reduction of $BrONO_2$ over northern Europe and northern Russia. Figure 11b shows that BrO is now the dominant bromine species in the sunlit atmosphere over Scandinavia with a peak mixing ratio of 7 pptv. In the region of perturbed air which is in darkness, BrCl is the main nighttime reservoir (not shown). A latitude height cross section at 50°E of BrO is shown in Figure 12 for 1200 UT on February 6th. The region of PSC-perturbed chemistry in the Arctic lower stratosphere is clearly marked, with elevated BrO levels between 50-70°N and 100-20 hPa. At 80 hPa (approximately θ=400 K) there is a very strong vertical gradient of BrO which increases to over 7 pptv between 60-20 hPa (approximately θ=440-580 K). During the AASE, *Toohey et al.* [1990] measured BrO mixing ratios of 4±2 pptv at θ=400 K rising to 8±2 pptv at θ=470 K, which is in agreement with the model. The integrated column of BrO in the model tends to underestimate the available observations, however. During the AASE *Wahner et al.*, [1990] generally measured vertical BrO column densities from 2-5$x10^{13}$ molecules cm^{-2} and on one occasion measured a column of 13±4$x10^{13}$ molecules cm^{-2}. From Sondre Stromfjord *Perner et al.* [1991] measured vertical column BrO amounts of 4-9$x10^{13}$ molecules cm^{-2}. A plot of column BrO from run D is shown in Figure 11c. The maximum column is 2.2$x10^{13}$ molecules cm^{-2} which with a mixing ratio of BrO of 8 pptv at 30 hPa decreasing to 6 pptv at 70 hPa and 4 pptv at 100 hPa. The mixing ratio of inorganic bromine in the upper stratosphere in the model is 12 pptv, which is probably an underestimate.

Ozone Destruction. The model experiments have been analyzed to assess the the magnitude of the chemical ozone destruction that may have occurred during winter 1989-1990. Comparison of the model ozone from runs A and B gives an indication for the potential for ozone destruction in the vortex during the midwinter period. Figure 13 plots the difference in O_3 between run B and run A on the 500 K isentropic surface on the January 4 1990. There is very little ozone loss in run B; at the edge of the polar vortex peak destruction of 0.015 ppmv (an average of 1.5 ppbv/day) has occurred. The lack of sunlight at this time of year limits the destruction to a ring near the polar night terminator.

Comparison of runs C and D gives an estimate of the ozone destruction expected as a result of the PSC event of early February 1990. Throughout the period of these simulations the coldest stratospheric temperatures, where PSCs are possible, remained over northern Scandinavia and the northern Soviet Union. Thus circulation within the polar vortex would transport air through polar stratospheric

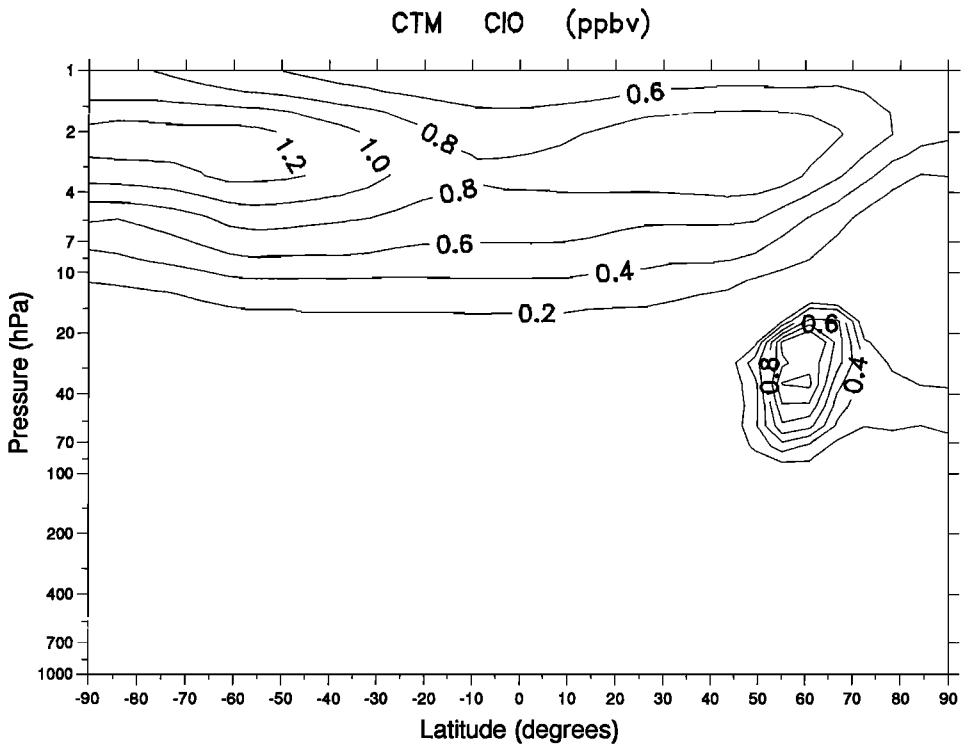

Fig. 10. Latitude cross section (at 50°E) of the mixing ratio of ClO (ppbv) from run D at 1200 UT on February 6. Contour interval is 0.2 ppbv.

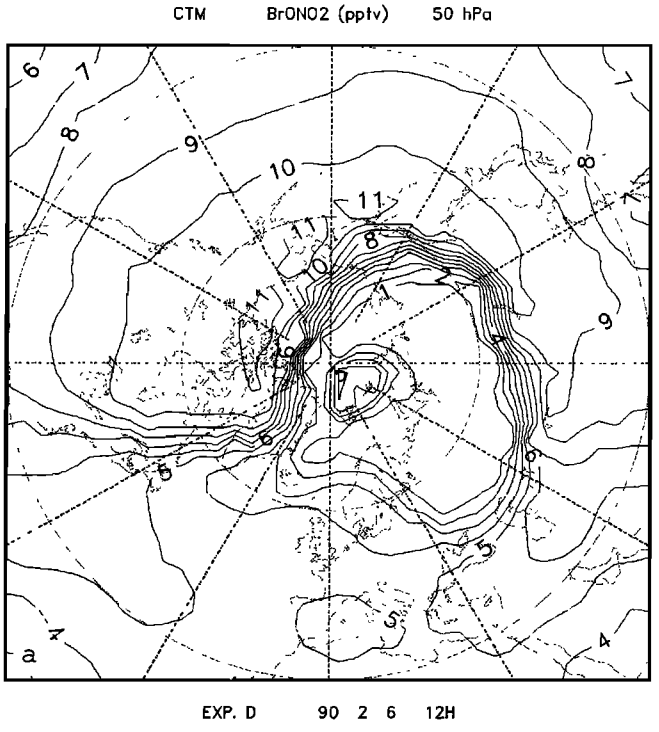

Fig. 11*a*. Mixing ratio of $BrONO_2$ (pptv) at 50 hPa at 1200 UT on February 6 from run D. Contour interval is 1 pptv.

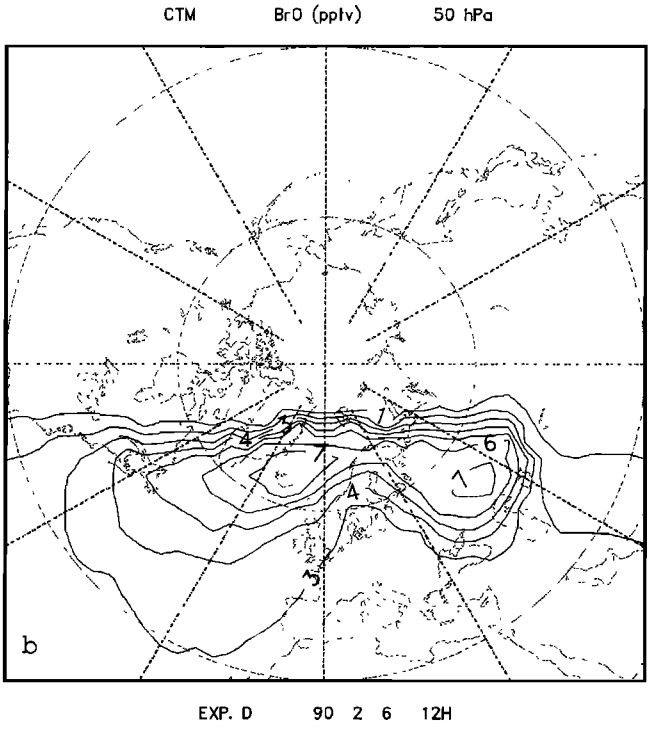

Fig. 11*b*. As Figure 11a but for BrO.

clouds implying that chemical O_3 destruction should be observed in and downwind of this region. Figure 14a plots the difference in O_3 mixing ratio between run C and run D at 50 hPa on February 14th. Within the polar vortex ozone destruction of up to 150 ppbv has occurred over 10 days; an average of 15 ppbv/day or around 0.75%/day. The corresponding loss in the column amount is around 7 DU (Figure 14b). Despite the high levels of active chlorine in the model, the O_3 loss is still quite limited due to the low amount of sunlight in the northern polar region in early February. During winter 1989-1990 early February would have provided the best opportunity for the coincidence of

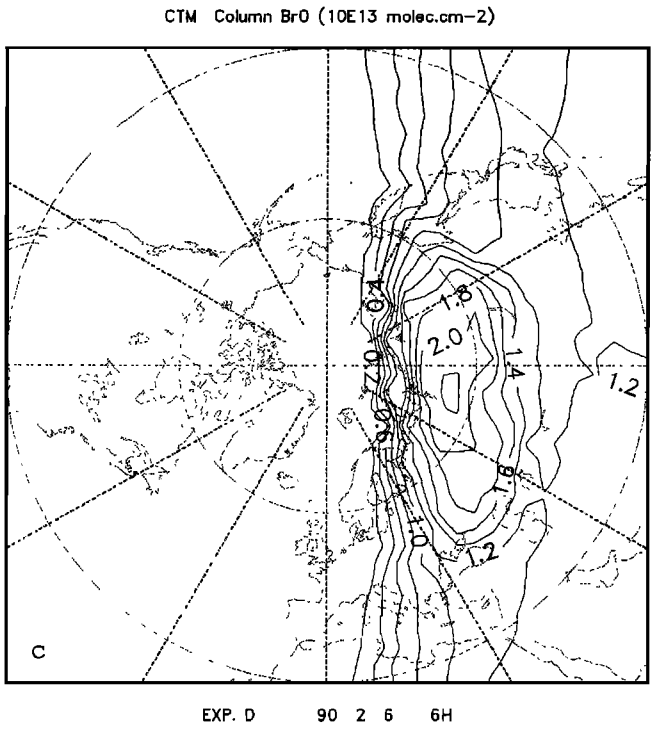

Fig. 11c. Column BrO ($x10^{13}$ molecules cm^{-2}) at 0600 UT on February 6 from run D.

PSC-processed air and sunlight. The relatively small magnitude of the ozone loss predicted in the model, compared to the variability of ozone induced by dynamics, highlights the problems in identifying the signature of chemical ozone loss in the Arctic.

Experiments E and F, which used the same dynamical forcing as experiments C and D, indicate the increased potential for ozone loss if PSCs persist until early March. Figure 15a shows that after 10 days ozone loss of 250 ppbv has occurred in the vortex at 50 hPa. The largest loss in the column (Figure 15b) is 14 DU near 70°N, 120°E. The local loss rate at 50 hPa of 25 ppbv/day (around 1.25%/day) in early March is similar to the rate of ozone loss observed at 18 km in early September in the Antarctic [*Anderson et al.*, 1991]. In the future significant ozone depletion could occur in the Arctic in winters with a late final warming.

An average ozone loss of 15 ppbv/day at 50 hPa in run D is similar to, but slightly less than that inferred by *Koike et al.* [1991]. It is also similar to the gradual trend seen by *Hofmann and Deshler* [1991] although it is much less than the rate of episodic loss inferred by them. The magnitude of ozone loss calculated with the model in early February (experiment D) is much less than that inferred by *Lefèvre et al.* [1991]. The large discrepancy between their model ozone field and the TOMS data is inconsistent with the chemical destruction mechanisms analyzed here. Model run D used the same initial conditions for ozone and the meteorological variables as the high resolution (T79) experiments of *Lefèvre et al* [1991] and *Riishojgaard et al.* [1992]. Overall, when compared to TOMS data (not shown), the evolution of the column ozone in run D is poorer than that by *Riishojgaard et al.* [1992], as would be expected with the lower resolution of T21. However, the gross features in the model ozone field are similar as the experiments were performed with essentially the same dynamical model. *Lefèvre et al* (1991) argued that the initial ozone field synthesized from TOMS data provides a good estimate of the profile. If the evolution of the model dynamics is realistic then this would suggest that the large discrepancy in the ozone column between their T79 experiments and the TOMS data over central Siberia is due either to an underestimate by the TOMS instrument or a rapid, as yet unknown, chemical ozone sink. However,

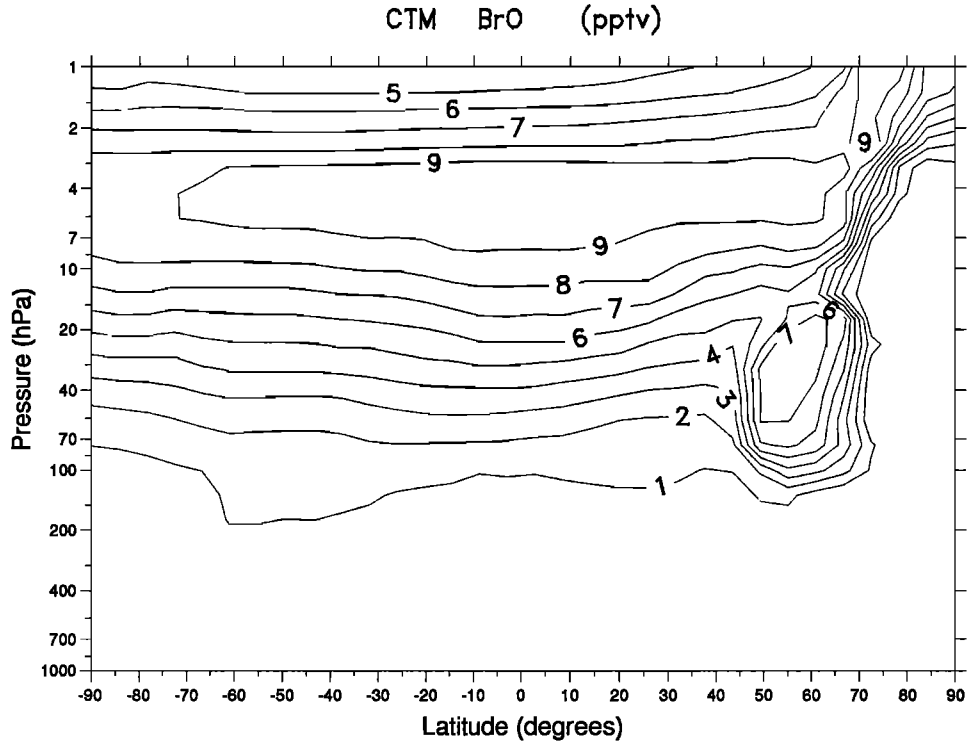

Fig. 12. Latitude cross section (at 50°E) of the mixing ratio of BrO (pptv) from run D at 1200 UT on February 6. Contour interval is 1 pptv.

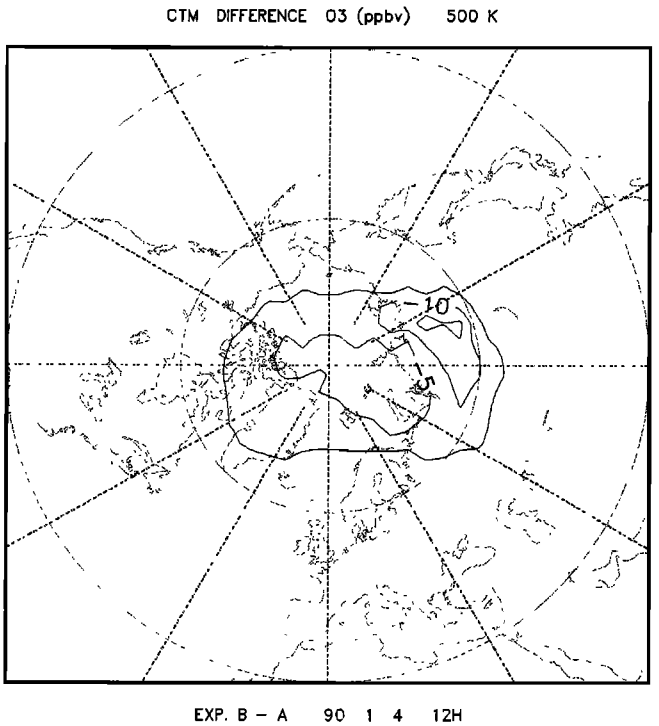

Fig. 13. The difference in O_3 mixing ratio (ppbv) between run B and run A on January 4 1990.

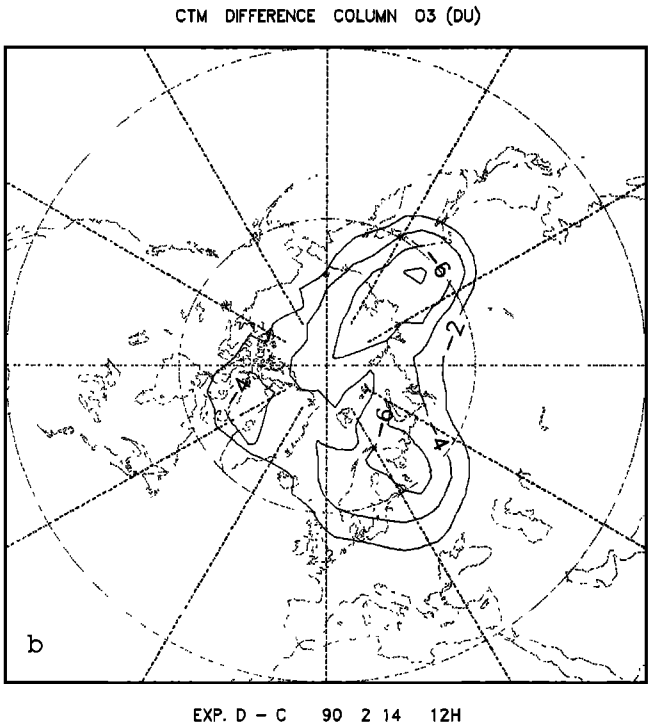

Fig. 14*b*. The difference in column O_3 (DU) between run D and run C on February 14 1990.

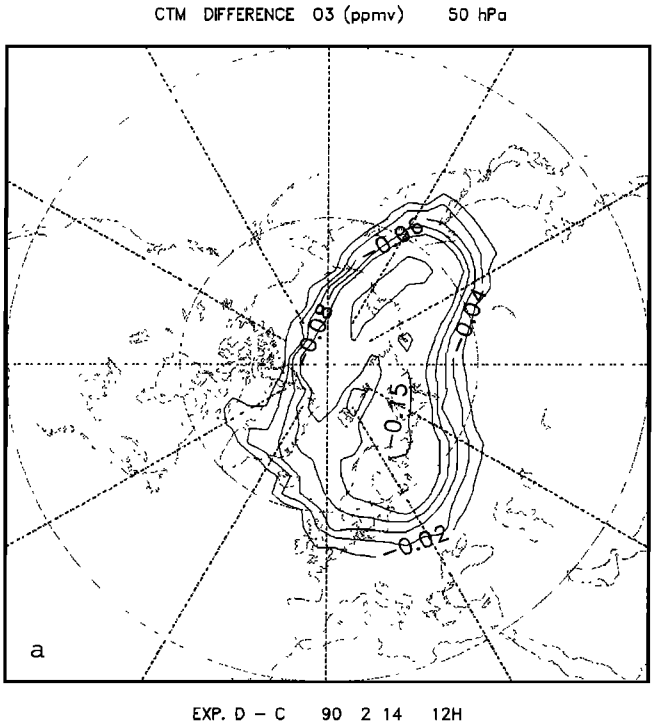

Fig. 14*a*. The difference in O_3 mixing ratio (ppmv) at 50 hPa between run D and run C on February 14 1990.

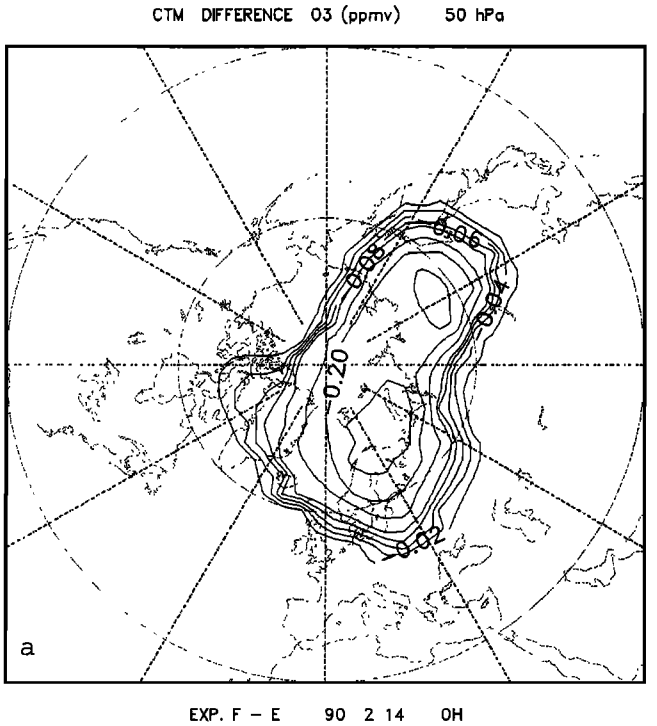

Fig. 15*a*. The difference in O_3 mixing ratio (ppmv) at 50 hPa between run F and run E on March 14 1990.

uncertainties in the reconstructed ozone profile could be the source of the discrepancy.

The chemical cycles responsible for this ozone destruction have been analyzed. *McKenna et al.* [1990] used results from an isentropic trajectory model at 470 K and concluded that the cycle involving ClO + ClO was by far the most significant loss cycle in early February. In the study of *McConnell et al.* [1991] loss due to the cycle involving ClO + O dominated at 20 km. *Murphy* [1991] used ER-2 data from the AASE campaign to calculate the expected loss due to the cycles involving ClO + ClO and ClO + BrO over the aircraft flight range. We have used our 3D model results to investigate how the efficiencies of these catalytic cycles vary with altitude, latitude and time. The model conti-

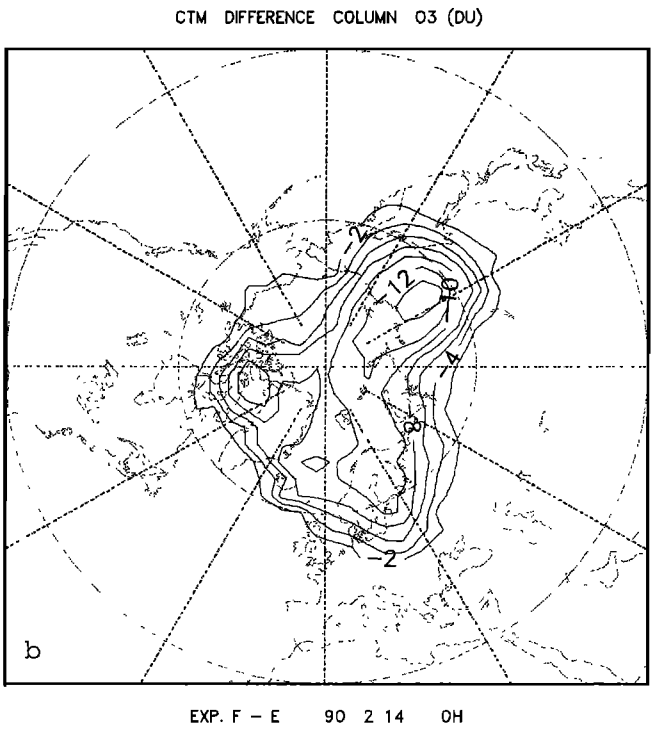

Fig. 15*b*. The difference in column O_3 (DU) between run F and run E on March 14 1990.

nuity equation for O_x was combined with the steady state expressions used to partition the model families to identify the rate determining steps in the important catalytic cycles [*Johnston and Podolske*, 1978]. In model runs D and F the following cycles dominate the ozone loss in the polar lower stratosphere:

Cycle I

$$ClO + ClO + M \rightarrow Cl_2O_2 + M$$
$$Cl_2O_2 + h\nu \rightarrow ClO_2 + Cl$$
$$ClO_2 + M \rightarrow Cl + O_2 + M$$
$$2(Cl + O_3 \rightarrow ClO + O_2)$$
$$\text{net} : 2O_3 \rightarrow 3O_2$$

Cycle II

$$ClO + BrO \rightarrow Cl + Br + O_2$$
$$Cl + O_3 \rightarrow ClO + O_2$$
$$Br + O_3 \rightarrow BrO + O_2$$
$$\text{net} : 2O_3 \rightarrow 3O_2$$

Cycle II can also be initialized by the formation and subsequent photolysis of BrCl.

Cycle III

$$ClO + O \rightarrow Cl + O_2$$
$$Cl + O_3 \rightarrow ClO + O_2$$
$$\text{net} : O + O_3 \rightarrow 2O_2$$

Cycle IV

$$ClO + HO_2 \rightarrow HOCl + O_2$$
$$HOCl + h\nu \rightarrow OH + Cl$$
$$Cl + O_3 \rightarrow ClO + O_2$$
$$OH + O_3 \rightarrow HO_2 + O_2$$
$$\text{net} : 2O_3 \rightarrow 3O_2$$

The other catalytic cycles make a minor contribution to the ozone loss. *Bekki et al.* [1991] noted that in the presence of heterogeneous chemistry on sulphate aerosols ozone loss in the lower stratosphere is controlled mostly by HO_x chemistry. The "chronic" effects of heterogeneous processing on sulphate aerosols can be contrasted with the "acute" effect of processing by PSCs where ozone loss is dominated by the ClO and BrO radicals. Figure 16 plots the ozone loss due to cycle I in early February and early March. In general, this cycle is the dominant loss cycle in both runs D and F throughout the winter. In early February (Figure 16a) the maximum instantaneous loss rate (at about 1500 local time) is 50 ppbv/day centered at 60°N and between 35 and 50 hPa. By early March the peak loss rate is over 75 ppbv/day. The efficiency of cycle I increases at low altitudes as it is initiated by the three-body formation of Cl_2O_2. At altitudes below 60 hPa the efficiency of the catalytic cycles is limited by the availability of active chlorine (see Figure 10) which in turn is limited by the total inorganic chlorine. It is ozone destruction at the lower altitudes which will have the largest impact on the integrated column amount. Figure 17 shows the ozone loss due to cycle II. In early February the maximum loss is 25 ppbv/day at around 30-50 hPa at 55°N. Thus the peak destruction due to cycle II is about 50% of that due to cycle I. The importance of cycle II could

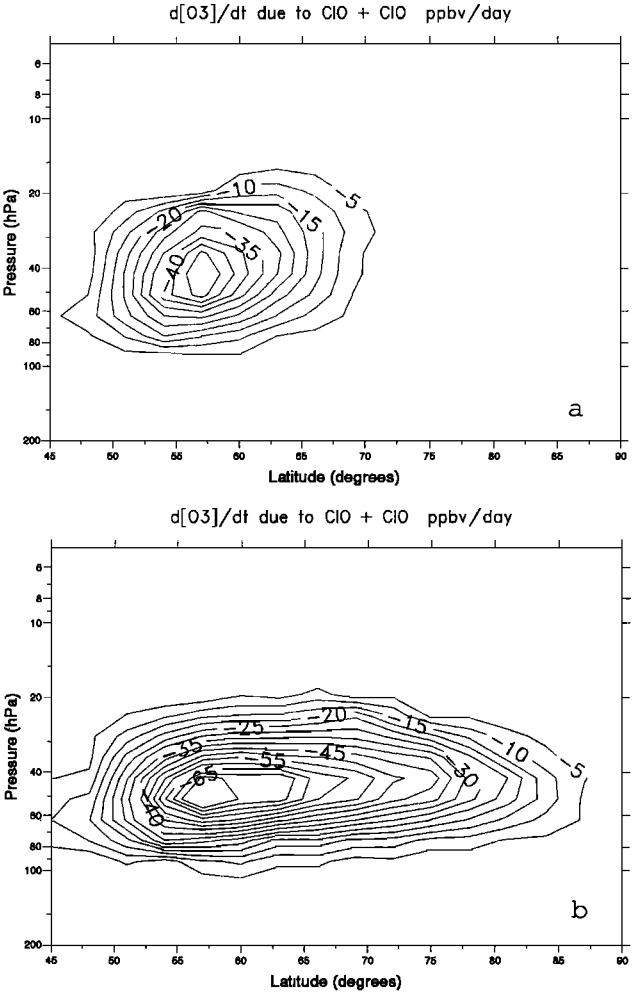

Fig. 16. Instantaneous rate of loss of O_3 (ppbv/day) at 50°E at 1200 UT (about 1500 local time) due to catalytic cycle I for a) February 6 from run D and b) March 6 from run F.

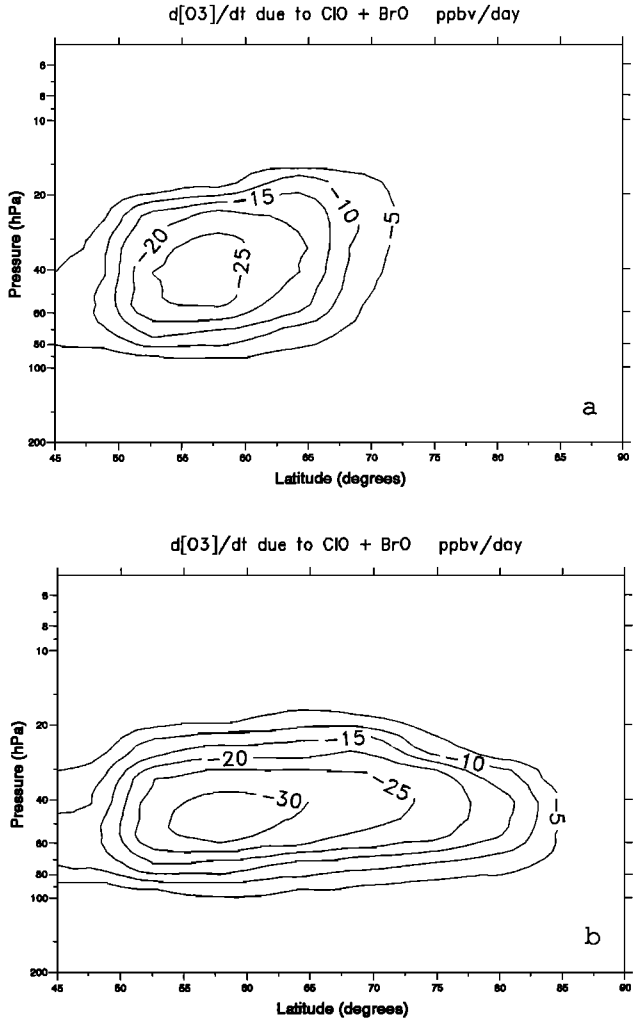

Fig. 17. As Figure 16 but for cycle II.

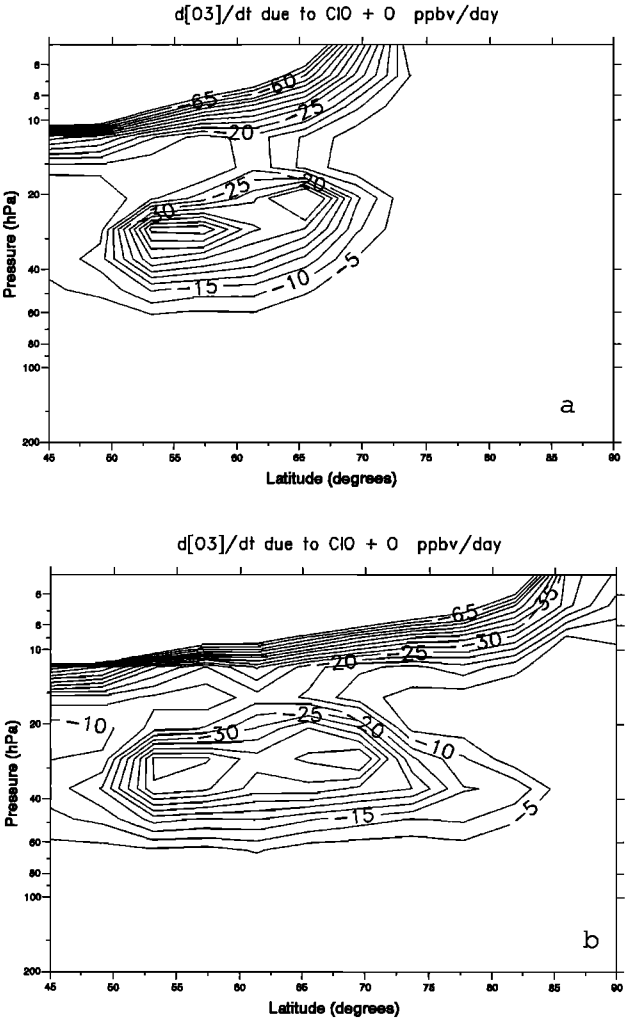

Fig. 18. As Figure 16 but for cycle III (N.B. contours stop at -80).

be underestimated, however, as the model runs contained a peak stratospheric mixing ratio of inorganic bromine of 12 pptv. By early March the loss due to cycle II has only increased to just over 30 ppbv/day. Now the contribution of cycle II is less compared to cycle I (about 40%). Although the rate of ozone loss due to cycle I is much greater than that due to cycle II at the peak of the ClO mixing ratio (Figure 10) near the periphery of the region of elevated ClO and BrO (Figure 12) loss due to the two cycles is similar. The location of the -10 ppbv/day contour is essentially the same in Figures 16a and 17a. The peak in BrO mixing ratio is much broader than the peak in ClO mixing ratio. Ozone loss due to cycle III is plotted in Figure 18. In early February the peak ozone loss rate is 55 ppbv/day situated around 28 hPa and 53-57°N. At 50 hPa the loss due to cycle III is only 10-15 ppbv/day. Thus when expressed as the mixing ratio loss, cycle III can destroy ozone at a rate comparable to, or even greater than, cycle I. However, the destruction due to cycle III is a maximum above 30 hPa due to the rapid increase of atomic oxygen with altitude. Ozone loss at around 20-30 hPa will have less of an effect on the column and can also be compensated for, to some extent, by in situ production of odd oxygen (see below). By early March the maximum ozone loss due to cycle III is still around 50 ppbv/day over a similar altitude range but now, due to the increased sunlight, loss occurs further towards the pole. Results for cycle IV are shown in Figure 19. In early February ozone loss due to this cycle is negligible. In early March the maximum loss of 25 ppbv/day occurs at around 30 hPa. The large increase in the efficiency of cycle IV reflects the increase in HO_2. In situ ozone production due to the photolysis of O_2 is shown in Figure 20. At altitudes above 30 hPa where cycle III is efficient at destroying ozone the photolysis of O_2 can compensate for the loss. At 30 hPa and 60°N in early March the rate of in situ ozone production is 30 ppbv/day. Climatology [e.g., *Barnett and Corney*, 1985] shows that temperatures are warmer in the Arctic winter stratosphere compared to the Antarctic. This limits the most likely occurrence of PSCs in the northern hemisphere to the altitude range 18-21 km (see, e.g. *World Meteorological Organisation/UNEP*, [1991]). In the southern hemisphere PSCs can commonly occur down to altitudes as low as 14 km and below. Therefore in the Arctic, chlorine activation by PSCs may be largely limited to higher altitudes than in the Antarctic where the efficiency of cycle I (the main cause of ozone loss in the Antarctic ozone hole) is reduced.

The evolution of the potential for ozone destruction by cycles I-III during the Arctic winter is illustrated by Figure 21. These data were calculated with a simple box model and shows the integrated amount of ozone destruction per day

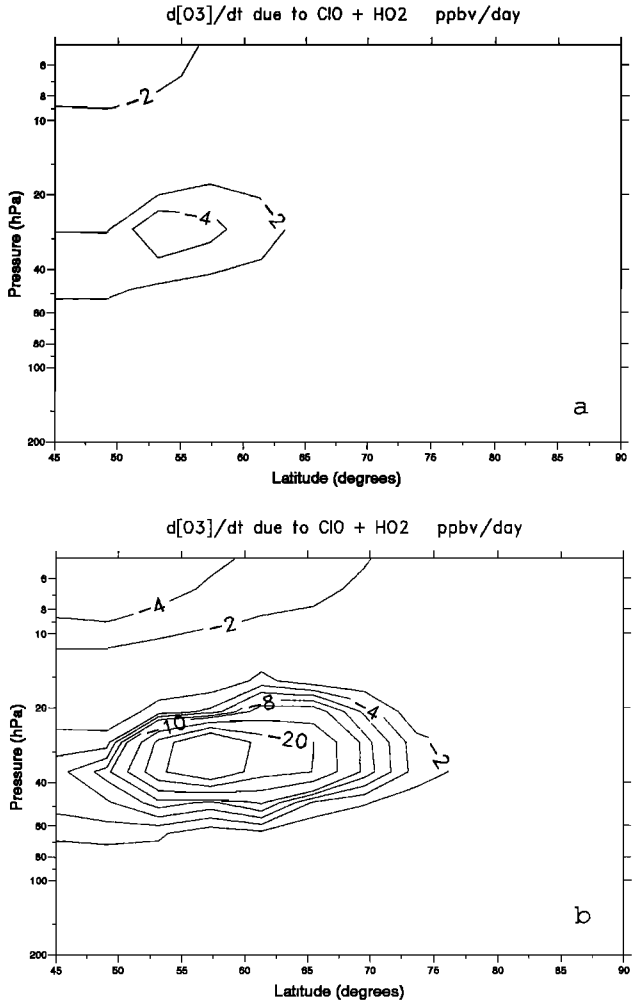

Fig. 19. As Figure 16 but for cycle IV.

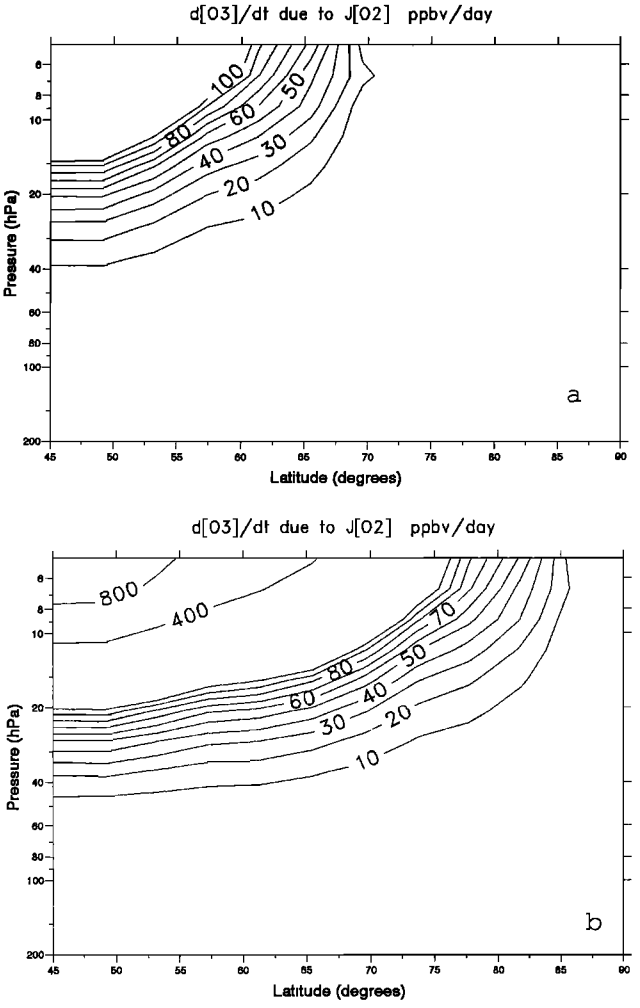

Fig. 20. As Figure 16 but for production of odd oxygen by the photolysis of O_2 (N.B. irregular spacing of contours).

for these three cycles from January to March for an air parcel at 70°N and 50 hPa. The calculation assumes that the air parcel contains 1.5 ppbv of active chlorine and 10 pptv of BrO. During January the loss due to cycle I and cycle II is similar and increases to just under 2 ppbv/day at the end of the month. By the end of February, cycle 1 destroys 11-12 ppbv/day and by the end of March over 20 ppbv/day. Destruction by cycle II increases to 13 ppbv/day by the end of March. Also shown in the figure is the hours of sunlight per day at this point in the atmosphere. The efficiency of cycle I increases more rapidly over this period than cycles II and III. As the concentration of daytime BrO is effectively constant in the box the increase in ozone destruction due to cycle II reflects the shift of the ClO_x equilibrium from Cl_2O_2 to ClO as the intensity of sunlight increases and also the increasing amount of daylight. Similarly, as the concentration of O atoms at this altitude is mainly controlled by photolysis of O_3 in the Chappuis band, where the atmosphere is optically thin, the mean daytime O concentration will not change by much over this period. The increase in O_3 loss due to cycle III therefore also reflects the increase in daytime ClO and the increasing amount of daylight. At altitudes above 30 hPa, where cycle III is most important, the balance between ClO and its dimer will be shifted more towards ClO as the intensity of sunlight is larger and the three-body formation of Cl_2O_2 is slower. Therefore the loss of ozone due to cycle III will depend almost entirely on the length of the day, as shown in Figure 18. The increase in ozone loss due to cycle I is faster due to the quadratic effect of the increase of daytime ClO on the rate of this cycle. Figure 21 illustrates the large increase in potential for ozone destruction if the polar vortex remains cold and stable beyond early February, the case in 1990. The increasing ozone destruction with time shown in the figure could also be achieved by the air parcel traveling equatorwards where more sunlight is available.

Figures 16-21 illustrate the different efficiencies for catalytic cycles in the destruction of ozone in the northern and southern polar regions. In the formation of the Antarctic ozone hole the O_3 loss occurs in September and is due mainly to the ClO dimer cycle with a minor role (25%) for bromine [*Anderson et al.*, 1991]. This season corresponds to March in the northern hemisphere where the dominance of cycle I is shown in Figures 16 and 21. However, by March temperatures are usually too warm for Arctic PSCs. In January and early February when Arctic PSCs are most common, the cycles involving BrO are relatively more important. However, for a strong Arctic ozone depletion, requiring PSCs to persist until late March, the ClO dimer will again be the most important cycle.

5. CONCLUSIONS

A three-dimensional radiative-dynamical-chemical model

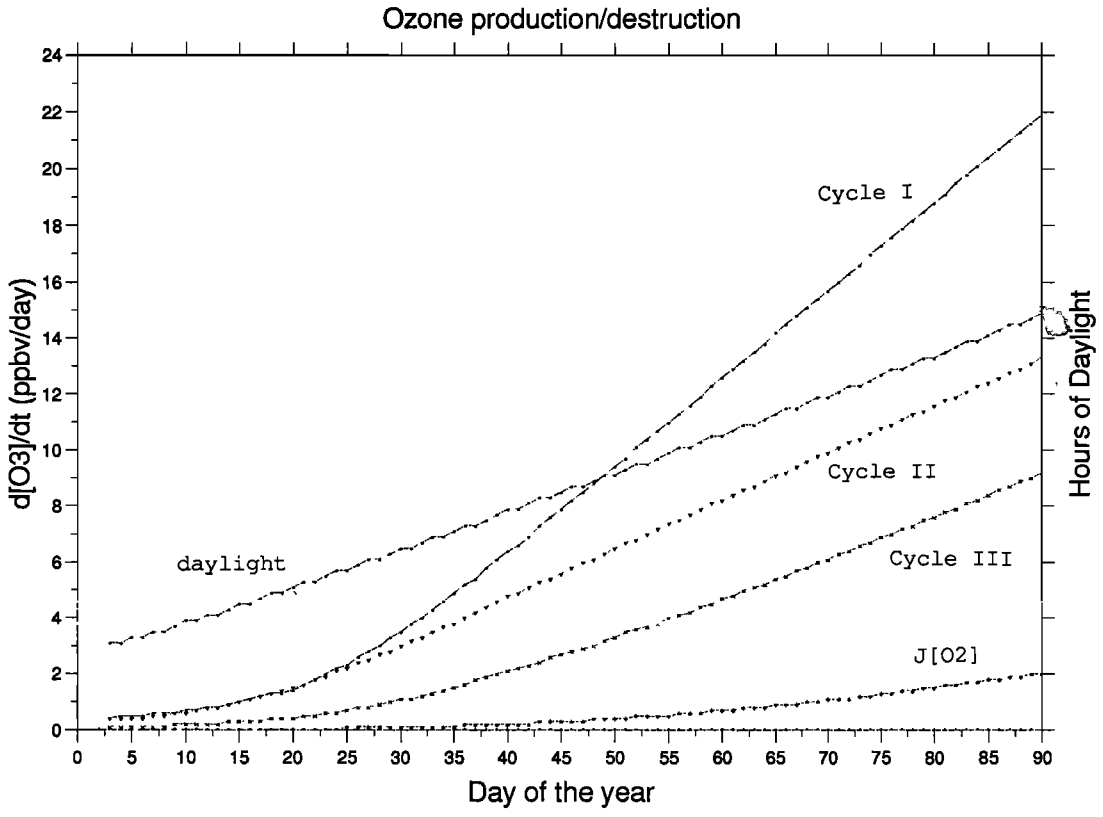

Fig. 21. Rate of loss of O_3 (ppbv/day) due to cycles I, II and III for an air parcel at 50 hPa, 70°N assuming a mixing ratio of ClO_x 1.5 ppbv, BrO 10 pptv, O_3 2.5 ppmv at T=200 K. Also shown is the rate of odd oxygen production due to the photolysis of O_2 and the number of hours of sunshine per day.

has been used to study the distribution of trace gases in the Arctic lower stratosphere during winter 1989-1990. The model was initialized using meteorological analyses of the ECMWF and using constituent data from a 2D model transformed into the coordinates of PV and θ. In some experiments TOMS data were used to initialize the model O_3 field. The model contains a comprehensive description of gas phase chemical reactions as well as a treatment of type I and type II polar stratospheric clouds. In the CTM the chemical species are transported using the second-order moments scheme of *Prather* [1986]. The use of this non diffusive scheme has resulted in a great improvement over the previous spectral scheme. This is particularly important in the comparatively low resolutions which the cost of 3D chemical transport models often necessitates.

A series of 10-day experiments were performed throughout the 1989-1990 winter. Type I PSCs would have begun to form around mid December. By the end of December the model predicts significant processing of air with a large reduction in HCl and an associated increase in active chlorine. The period of January 1990 was very cold with temperatures consistently below the threshold for the formation of type I PSCs in the polar vortex. In late January and early February type II PSCs were able to form. The chemical ozone loss produced in the model varied strongly with time through the amount of sunlight available. In early January the ozone loss (around 1.5 ppbv/day at 50 hPa) was small and confined to the edge of the vortex, near the terminator. In early February the rate of ozone loss in PSC-processed air was 15 ppbv/day (around 0.75%/day) at 50 hPa corresponding to a loss of just under 1DU/day from the column. In mid February 1990 temperatures became too warm for further PSC activity. If PSCs had persisted until early March ozone loss of around 25 ppbv/day at 50 hPa could have been sustained. In the future significant ozone depletion could occur for winters with late final warmings.

The cycles responsible for the destruction of O_3 have been analyzed using the 3D model results as a function of latitude, altitude and time. In general, the cycle initiated by the reaction ClO + ClO is the dominant loss mechanism below 30 hPa. However, early in January the cycles involving ClO + BrO become relatively more important. This would be especially true for BrO levels greater than 10 pptv. Also, where ClO levels are low, e.g., at the edge of the chemically perturbed region, the cycles involving bromine will play a relatively more important role. Later in the season (corresponding to the conditions in which the Antarctic ozone hole forms) the increasing intensity of sunlight, and the resultant shift of the equilibrium of Cl_2O_2 to ClO greatly increases the efficiency of the ClO + ClO cycle. At altitudes above 30 hPa the cycle involving the reaction ClO + O is most efficient at destroying ozone. At these altitudes some in situ compensation for the O_3 loss can occur through the photolysis of O_2.

A number of trace species in the model have been compared with the available observations. In particular, results from the model are in accord with the ground based observations of HNO_3, NO_2, HCl and OClO. The model (with 12 pptv of inorganic bromine in the upper stratosphere) underestimates the measurements of the BrO column. The available measurements are, however, too sparse to effectively constrain the 3D model.

Although the results from the 3D model are encouraging and in agreement with observations a number of uncertainties remain. Short simulations of a 3D model are heavily influenced by the initial chemical conditions. Ideally, global constituent fields should be used to initialize and constrain the model. The experiments presented here were performed at the low horizontal resolution of T21 (about 5° x 5°) due to the computational expense of the detailed chemistry scheme. The winds and temperature used for the CTM were taken from a GCM simulation which also used the resolution of T21. In this low resolution the meteorological evolution of the model will diverge from reality quite quickly. A better forcing for the CTM would be obtained by using winds from a higher resolution GCM experiments or from assimilated data.

Acknowledgments. M.P.C. thanks NATO for funding a research fellowship which is administered by the U.K. Science and Engineering Research Council. This work was sponsored by the Programme Atmosphere Moyenne of the Centre National d'Etudes Spatiales, the Centre National de la Recherche Scientifique and the Ministère de l'Environnement (under grant 91-100), and by the Commission of the European Communities (under STEP project 016).

REFERENCES

Abbatt, J. P. D., K. D. Beyer, A. F. Fucaloro, J. R. McMahon, P. J. Wooldridge, R. Zhang, and M. J. Molina, Interaction of HCl vapor with water-ice: Implications for the Stratosphere, *J. Geophys. Res.*, *97*, 15,819-15826, 1992.

Adrian, G. P., T. Blumenstock, H. Fischer, L. Gerhardt, T. Gulde, H. Oelhaf, P. Thomas, and O. Trieschmann, Column amounts of trace gases derived from ground-based measurements with MIPAS during CHEOPS III, *Geophys. Res. Lett.*, *18*, 783-786, 1991.

Anderson, J. G., D. W. Toohey and W. H. Brune, Free radicals within the Antarctic vortex: The role of CFC's in the Antarctic ozone loss, *Science*, *251*, 39-46, 1991.

Austin, J., R. R. Garcia, J. M. Russell III, S. Solomon, and A. F. Tuck, On the atmospheric photochemistry of nitric acid, *J. Geophys. Res.*, *91*, 5477-5485, 1986.

Barnett, J. J., and M. Corney, Middle atmosphere reference model derived from satellite data, Middle Atmosphere Program, Handbook for MAP, vol. 16, pp. 47-85, Scientific Committee on Solar-Terrestrial Physics (SCOSTEP), Copies available from SCOSTEP Secretariat, University of Illinois, 1985.

Bekki, S., R. Toumi, J. A. Pyle, and A. E. Jones, Future aircraft and global ozone, *Nature*, *354*, 193-194, 1991.

Cariolle, D., and D. Brard, The distribution of ozone and other active species : results of a two-dimensional model, in *Procedings of the Quadrennial Ozone Symposium*, edited by R. D. Bojkov and P. Fabian, Halkidiki, pp77-81, D. Reidel, Dordrecht, 1984.

Cariolle, D., A. Lasserre-Bigorry, J. F. Royer, and J. F. Geleyn, A general circulation model simulation of the springtime Antarctic ozone decrease and its impact on mid-latitudes, *J. Geophys. Res.*, *95*, 1883-1898, 1990.

DeMore, W.B., et al, Chemical kinetics and photochemical data for use in stratospheric modeling, Evaluation no. 9, NASA/JPL Publ. 90-1, Jet Propul. Lab., Pasadena, Calif., 1990.

Douglass, A. R., R. B. Rood, R. S. Stolarski, M. R. Schoeberl, M. H. Proffitt, J. J. Margitan, M. Loewenstein, J. R. Podolske, and S. E. Strahan, Global three-dimensional constituent fields derived from profile data, *Geophys. Res. Lett.*, *17*, 525-528, 1990.

Douglass, A. R., R. B. Rood, J. A. Kaye, R. S. Stolarski, D. J. Allen and E. M. Larson, The influence of polar stratospheric heterogeneous processes on reactive chlorine at middle latitudes: Three-dimensional model implications, *Geophys. Res. Lett.*, *18*, 25-28, 1991.

Granier, C., and G. Brasseur, Ozone and other trace gases in the Arctic and Antarctic regions: Three-dimensional model simulations, *J. Geophys. Res.*, *96*, 2995-3011, 1991.

Hanson, D., and K. Mauersberger, Laboratory studies of the nitric acid trihydrate: Implications for the south polar stratosphere, *Geophys. Res. Lett.*, *15*, 855-858, 1988a.

Hanson, D., and K. Mauersberger, Solubility and equilibrium vapor pressures of HCl dissolved in polar stratospheric cloud material: Ice and the trihydrate of nitric acid, *Geophys. Res. Lett.*, *15*, 1507-1510, 1988b.

Harwood R. S. and J. A. Pyle, A two-dimensional mean circulation model for the atmosphere below 80km, *Q. J. R. Meteol. Soc.*, *101*, 723-748, 1975.

Hofmann, D. J., and T. Deshler, Evidence from balloon measurements for chemical ozone depletion of stratospheric ozone in the Arctic winter of 1989-90, *Nature*, *349*, 300-305, 1991.

Johnston, H. S., and J. Podolske, Interpretation of stratospheric photochemistry, *Rev. Geophys.*, *16*, 491-519, 1978.

Kaye, J. A., A. R. Douglass, R. B. Rood, R. S. Stolarski, P. A. Newman, D. J. Allen, and E. M. Larson, Spatial and temporal variability of the extent of chemically processed stratospheric air, *Geophys. Res. Lett.*, *18*, 29-32, 1991.

Koike, M., Y. Kondo, M. Hayashi, Y. Iwasaka, P. A. Newman, M. Helten, and P. Aimedieu, Depletion of Arctic ozone in the winter 1990, *Geophys. Res. Lett.*, *18*, 791-794, 1991.

Lary, D. J., and J. A. Pyle, Diffuse radiation, twilight and photochemistry, *J. Atmos. Chem.*, *13*, 373-392, 1991.

Lefèvre, F., L. P. Riishojgaard, D. Cariolle, and P. Simon, Modelling the February 1990 PSC type II event and its potential impact on the Northern hemisphere ozone content, *J. Geophys. Res.*, *96*, 22,509-22,534, 1991.

McConnell, J. C., W. F. J. Evans and E. M. J. Templeton, Model simulation of chemical depletion of Arctic ozone during the winter of 1989, *J. Geophys. Res.*, *96*, 10,923-10,930, 1991.

McKenna, D. S., R. L. Jones, L. R. Poole, S. Solomon, D. W. Fahey, K. K. Kelly, M. H. Proffitt, W. H. Brune, M. Loewenstein, and K. R. Chan, Calculation of ozone destruction during the 1988/89 Arctic winter, *Geophys. Res. Lett.*, *17*, 553-556, 1990.

Muller, R., The performance of classical versus modern finite one-dimensional test-bed, *Mon. Weather Rev.*, *120*, 1407-1415, 1992.

Murphy, D. M., Ozone loss rates calculated along ER-2 flight tracks, *J. Geophys. Res.*, *96*, 5045-5053, 1991.

Murray, F. W., On the computation of saturation vapor pressure, *J. Appl. Meteorol.*, *6*, 203-204, 1967.

Naujokat, B., K. Labitzke, R. Lenschow, K. Petzoldt, and R.-C. Wohlfart, The stratospheric winter of 1989/90: Very cold with a pronounced minor warming and a late final warming, *Beil. Berl. Wetterkarte*, *75/90, SO12/90*, Freien Universitat Berlin, 1990.

Perner, D., T. Klupfel, U. Parchatka, A. Roth, and T. Jorgensen, Ground based UV-vis spectroscopy: Diurnal OClO profiles during January 1990 above Sondre Stromfjord, Greenland, *Geophys. Res. Lett.*, *18*, 787-790, 1991.

Pommereau, J. P., F. Goutail, and A. Sarkissan, Observations de la stratosphere par spectrometrie UV-visible depuis le sol, PAMOY CHEOPS III, final report, edited by J. P. Pommereau, Verrieres le Buisson, 1991.

Pommereau, J. P., and U. Schmidt, CHEOPS III: An ozone research campaign in the Arctic winter stratosphere 1989/90, *Geophys. Res. Lett.*, *18*, 759-762, 1991.

Prather, M. J., Numerical advection by conservation of second-order moments, *J. Geophys. Res.*, *91*, 6671-6681, 1986.

Prather, M., and A. H. Jaffe, Global Impact of the Antarctic ozone hole: chemical propagation, *J. Geophys. Res.*, *95*, 3473-3492, 1990.

Ramaroson, R. A., Modelisation locale, a une et trois dimensions des processus photochimiques de l'atmosphere moyenne, Ph.D. thesis, Univ. Paris VI, 1989.

Ramaroson, R., D. Cariolle and M. Pirre, Simulation of Noxon cliff in a three-dimensional model with diurnal variations during an unperturbed winter, Polar Stratospheric Ozone, in *Proceedings of the First European Workshop, 3-5 October 1990, Schliersee*, FRG, edited by J. A. Pyle and N. R. P. Harris, pp267-270, Commission of the European Communities, 1990.

Ramaroson, R., M. Pirre, and D. Cariolle, A box model for on-line computations of diurnal variations in a 1D model: Potential for application to multidimensional cases, *Ann. Geophys.*, *10*,

416-428, 1992.

Rattigan, O., E. Lutman, R. L. Jones, R. A. Cox, K. Clemitshaw, and J. Williams, Temperature dependent absorption cross sections of gaseous nitric acid and methyl nitrate, *J. Photochem. Photobiol. A*, *66*, 313-326, 1992.

Riishojgaard, L. P., F. Lefevre, D. Cariolle, and P. Simon, A GCM simulation of the northern hemisphere ozone field in early February 1990 using satellite total ozone for model initialisation, *Ann. Geophys.*, *10*, 54-74, 1992.

Rodriguez, J. M. et al., Nitrogen and chlorine species in the spring Antarctic stratosphere: Comparison of models with airborne Antarctic ozone experiment observations, *J. Geophys. Res.*, *94*, 16,6883-16,703, 1989.

Rood, R. B., J. A. Kaye, A. R. Douglass, D. J. Allen, S. Steenrod and E. M. Larson, Wintertime nitric acid chemistry: Implications from three-dimensional model calculations, *J. Atmos. Sci.*, *47*, 2696-2709, 1990.

Rood, R. B., J. E. Nielsen, R. S. Stolarski, A. R. Douglass, J. A. Kaye, and D. J. Allen, Episodic total ozone minima and associated effects of heterogeneous chemistry and lower stratospheric transport, *J. Geophys. Res.*, *97*, 7979-7996, 1992.

Salawitch, R. J., et al, Loss of ozone in the Arctic vortex for the winter of 1989, *Geophys. Res. Lett.*, *17*, 561-564, 1990.

Schiller, C., A. Wahner, U. Platt, H.-P. Dorn, J. Callies, and D. H. Ehalt, Near uv atmospheric absorption measurements of column abundances during airborne Arctic stratospheric expedition, January - February 1989, 2, OClO observations, *Geophys. Res. Lett.*, *17*, 501-504, 1990.

Schmidt, U., R. Bauer, A. Khedim, E. Klein, G. Kulessa, and C. Schiller, Profile observations of long-lived trace gases in the Antarctic vortex, *Geophys. Res. Lett.*, *18*, 767-770, 1991.

Schoeberl, M. R., M. H. Proffitt, K. K. Kelly, L. R. Lait, P. A. Newman, J. E. Rosenfield, M. Loewenstein, J. R. Podolske, S. E. Strahan, and K. R. Chan, Stratospheric constituent trends derived from ER-2 profile data, *Geophys. Res. Lett.*, *17*, 469-472, 1990.

Solomon, S., Progress towards a quantitative understanding of Antarctic ozone depletion, *Nature*, *347*, 347-354, 1990.

Solomon S., G. H. Mount, R. W. Sanders, R. O. Jakoubek, and A. L. Schmeltekopf, Observations of the nighttime abundance of OClO in the winter stratosphere above Thule, Greenland, *Science*, *242*, 550-555, 1988.

Toohey, D. W., J. G. Anderson, W. H. Brune and K. R. Chan, In situ measurements of BrO in the Arctic stratosphere, *Geophys. Res. Lett.*, *17*, 513-516, 1990.

Wahner, A., J. Callies, H. P. Dorn, U. Platt, and C. Schiller, Near UV atmospheric absorption measurements of column abundances during Airborne Arctic Stratospheric Expedition, January - February 1989, 3, BrO Observations, *Geophys. Res. Lett.*, *17*, 517-520, 1990.

World Meteorological Organisation/UNEP, Scientific assessment of ozone depletion, Global Ozone Research and Monitoring Project, *Rep. 25*, Geneva, 1991.

D. Cariolle and P. Simon, Météo France, Centre National de Recherches Météorologiques, 42 Ave. Coriolis, 31057 Toulouse, France.

M. Chipperfield and D. J. Lary, Centre for Atmospheric Science, Department of Chemistry, University of Cambridge, Lensfield Rd., Cambridge, CB2 1EW, U.K.

R. Ramaroson, Office National d'Etudes et de Recherches Aérospatiales, 92322 Châtillon, France.

(Received December 30, 1991;
revised December 15, 1992;
accepted December 15, 1992)